NAVAL POSTGRADUATE SCHOOL

MONTEREY, CALIFORNIA

THESIS

THE FREQUENCY RESPONSE, IMPULSE RESPONSE AND TRANSFER FUNCTION OF AN OCEAN WAVEGUIDE

by

Walter B. Schulte III

June 2004

Thesis Advisor:	Lawrence J. Ziomek
Second Reader:	Roberto Cristi

Approved for public release; distribution is unlimited

THIS PAGE INTENTIONALLY LEFT BLANK

REPORT DOCUMENTATION PAGE			Form Approved OMB No. 0704-0188
Public reporting burden for this collection of information is estimated to average 1 hour per response, including the time for reviewing instruction, searching existing data sources, gathering and maintaining the data needed, and completing and reviewing the collection of information. Send comments regarding this burden estimate or any other aspect of this collection of information, including suggestions for reducing this burden, to Washington headquarters Services, Directorate for Information Operations and Reports, 1215 Jefferson Davis Highway, Suite 1204, Arlington, VA 22202-4302, and to the Office of Management and Budget, Paperwork Reduction Project (0704-0188) Washington DC 20503.			
1. AGENCY USE ONLY ***(Leave blank)***	**2. REPORT DATE** June 2004	**3. REPORT TYPE AND DATES COVERED** Master's Thesis	
4. TITLE AND SUBTITLE: The Frequency Response, Impulse Response, and Transfer Function of an Ocean Waveguide			**5. FUNDING NUMBERS**
6. AUTHOR Walter Barry Schulte III			
7. PERFORMING ORGANIZATION NAME(S) AND ADDRESS(ES) Naval Postgraduate School Monterey, CA 93943-5000			**8. PERFORMING ORGANIZATION REPORT NUMBER**
9. SPONSORING /MONITORING AGENCY NAME(S) AND ADDRESS(ES) N/A			**10. SPONSORING/MONITORING AGENCY REPORT NUMBER**
11. SUPPLEMENTARY NOTES The views expressed in this thesis are those of the author and do not reflect the official policy or position of the Department of Defense or the U.S. Government.			
12a. DISTRIBUTION / AVAILABILITY STATEMENT Approved for public release; distribution is unlimited			**12b. DISTRIBUTION CODE**

13. ABSTRACT (maximum 200 words)

In this thesis, the ocean was modeled as a waveguide with an ideal pressure – release surface, and an ideal rigid bottom. The ocean waveguide was then treated as a linear, time – invariant, space – variant (TISV) filter or communication channel. The filter is time – invariant because no motion was modeled and because the properties of the ocean were assumed to be constant. The filter is space – variant because of the presence of the two boundaries, that is, the ocean surface and ocean bottom.

This thesis investigates the ocean as a linear TISV filter by evaluating 1) the complex frequency response, 2) the impulse response, and 3) the transfer function of the ocean with respect to depth. It is shown that the TISV impulse response of the ocean contains information that can be used to help localize a target in range and whether the target is above or below the receiver. Computer simulation results were obtained by evaluating the three filter functions for several different test cases.

14. SUBJECT TERMS Anti – submarine warfare; ideal pressure – release surface, rigid bottom ocean waveguide model; linear, time – invariant, space – variant filters; complex frequency response, impulse response, and transfer function of the ocean; target localization			**15. NUMBER OF PAGES** 65 **16. PRICE CODE**
17. SECURITY CLASSIFICATION OF REPORT Unclassified	**18. SECURITY CLASSIFICATION OF THIS PAGE** Unclassified	**19. SECURITY CLASSIFICATION OF ABSTRACT** Unclassified	**20. LIMITATION OF ABSTRACT** UL

NSN 7540-01-280-5500 Standard Form 298 (Rev. 2-89)
Prescribed by ANSI Std. 239-18

THIS PAGE INTENTIONALLY LEFT BLANK

Approved for public release, distribution is unlimited

THE FREQUENCY RESPONSE, IMPULSE RESPONSE, AND TRANSFER FUNCTION OF AN OCEAN WAVEGUIDE

Walter B. Schulte III
Ensign, United States Navy
Electrical Engineering (B.S.), University of California, Los Angeles, 2003

Submitted in partial fulfillment of the
requirements for the degree of

MASTER OF SCIENCE IN APPLIED SCIENCE (SIGNAL PROCESSING)

from the

NAVAL POSTGRADUATE SCHOOL
June 2004

Author: Walter B. Schulte III

Approved by: Dr. Lawrence J. Ziomek
Thesis Advisor

Dr. Roberto Cristi
Second Reader

Dr. Donald Brutzman
Chairman, Under Sea Warfare Academic Committee

THIS PAGE INTENTIONALLY LEFT BLANK

ABSTRACT

In this thesis, the ocean was modeled as a waveguide with an ideal pressure – release surface, and an ideal rigid bottom. The ocean waveguide was then treated as a linear, time – invariant, space – variant (TISV) filter or communication channel. The filter is time – invariant because no motion was modeled and because the properties of the ocean were assumed to be constant. The filter is space – variant because of the presence of the two boundaries, that is, the ocean surface and ocean bottom.

This thesis investigates the ocean as a linear TISV filter by evaluating 1) the complex frequency response, 2) the impulse response, and 3) the transfer function of the ocean with respect to depth. It is shown that the TISV impulse response of the ocean contains information that can be used to help localize a target in range and whether the target is above or below the receiver. Computer simulation results were obtained by evaluating the three filter functions for several different test cases.

THIS PAGE INTENTIONALLY LEFT BLANK

TABLE OF CONTENTS

THIS PAGE INTENTIONALLY LEFT BLANK

LIST OF FIGURES

LIST OF TABLES

THIS PAGE INTENTIONALLY LEFT BLANK

ACKNOWLEDGMENTS

I would like to thank Dr. Ziomek and Dr. Cristi for their time and effort in advising me on this thesis.

THIS PAGE INTENTIONALLY LEFT BLANK

I. INTRODUCTION

This chapter provides a discussion of ocean waveguide modeling. This discussion will begin by presenting approaches taken by previous researchers. It will include a brief history of the topic, as well as the definition of the goals of the thesis and the approach taken to reach them. It also provides a brief summary of the mathematical framework used to describe ocean waveguide models.

A. HISTORY

The idea of treating the ocean as a communication channel has existed since the 1960s. For example, Ellinthorpe and Nuttall [1], Middleton [2], and Sostrand [3] proposed treating the ocean as a linear, time-varying, random filter. They proposed four filter functions for the ocean communication channel: the impulse response, the frequency response, the bi-frequency function, and the spreading function, as well as filter correlation functions for each. However, Ellinthorpe and Nuttall [1] and Middleton [2] refer to a transfer function rather than a frequency response. Similarly, in the 1970s, Laval [4,5], for example, proposed the idea of treating the ocean as a linear, time-varying, *space-varying* random filter. He used similar function definitions, and also discussed an angular spectrum function as well. Unfortunately, none generated mathematical expressions for these functions, and they remained in a purely theoretical state. Moreover, the terms "frequency response" and "impulse response" were not well defined in terms of linear, time-variant, space-variant (LTVSV) system theory. Another chief weakness of these filter-function models was that they were not related to solutions of a linear wave equation.

B. THE OCEAN AS A LINEAR, TIME-INVARIANT, SPACE-VARIANT (LTISV) FILTER

This thesis investigates treating the ocean as a linear, time-invariant, space-variant (LTISV) filter or communication channel. The ocean was modeled as a waveguide with an ideal pressure-release surface, and an ideal rigid bottom. The ocean - medium filter is assumed to be time-invariant because no motion was modeled and the properties of the ocean were assumed to be constant. The filter is space-variant because of the presence of the two boundaries, that is, the ocean surface and the ocean bottom. The time-invariant,

space-variant (TISV) complex frequency response of this ocean waveguide model is given in Ziomek[6]. It is based on solving the linear wave equation and satisfying all the boundary conditions associated with this ocean waveguide model. As shown in Ziomek [6], the TISV impulse response and TISV transfer function can be obtained from the TISV complex frequency response.

The goal of this thesis was to 1) evaluate the complex frequency response over a range of frequencies, 2) compute the corresponding impulse response, 3) derive and evaluate the corresponding transfer function, and 4) determine what information could be obtained from the three different filter functions. This thesis seeks to improve the understanding of ocean waveguides so that better algorithms for target localization in range and depth using either active or passive sonar can be obtained. This thesis will show that the impulse response function was the most informative in that respect. Once these functions were obtained, further restrictions were added to increase the relevance of the model to littoral combat. The ocean was restricted to a depth of 100 meters and the distance between source and receiver in the waveguide was assumed to be less than 1 kilometer.

C. DOD RELEVANCE

Since the end of the Cold War, the focus of the Navy has shifted from the deep ocean into the littoral areas. The littorals, as they are called, present unique complications for passive sonar that stem mostly from the interaction of sound signals with the ocean bottom and the ocean surface. The fact that sound can bounce off the bottom and surface causes much reverberation that is detected at the receiving sonar array. The reverberation is caused mostly by the multipath spreading in time due to the multiple bottom-surface interactions of sound rays, and the differing travel times of these rays. Moreover, since modern submarine-quieting techniques improve often, it is increasingly important to analyze transient, broadband signals. These broadband sources are often produced in an actual ocean environment for research purposes using an explosion. However, they can also be generated by a submarine opening a torpedo hatch door in a combat situation. Such transient noises may provide the only opportunity to locate modern, quieted submarines. Subsequently, it is necessary to obtain algorithms that exploit these noise sources for target localization in range and depth. This thesis

seeks to explore the behavior of a simulated broadband noise source in a shallow waveguide. It also seeks to demonstrate the possibility of locating the depth and range of such a noise source.

D. SUMMARY

Using the framework of linear filter theory, this thesis will explore the usefulness of three different ocean-medium filter functions. This thesis will show that the time-invariant, space-variant (TISV) impulse response of an ocean waveguide can be obtained from the inverse discrete Fourier transform of the corresponding TISV complex frequency response. It will then be shown that this impulse response yields information about the range and depth of the source emitting the impulse. The TISV transfer function will also be derived and evaluated to show the relationship between the magnitude response of an ocean waveguide and the angles of sound propagation from the source.

E. THESIS ORGANIZATION

This thesis is organized into five different chapters. Chapter I provides an overview of linear filter theory as applied to ocean waveguides, Navy relevance of the research, and goals for the thesis. Chapter II contains an overview of the three filter-functions and a discussion of numerical approximations. These approximations will be used to achieve the computational results presented in Chapter III. Chapter III contains the simulated results of the ocean waveguide for several different range and depth separations between the source and receiver. Chapter IV contains comparisons of the different cases and explanations of the results. Chapter V, the final chapter, contains thesis conclusions and recommendations for future research in ocean waveguide modeling.

THIS PAGE INTENTIONALLY LEFT BLANK

II. THE OCEAN AS A LINEAR FILTER

A. INTRODUCTION

As explained in Ziomek [6], this thesis uses the framework of linear filter theory to model the propagation of sound in the ocean. The assumption of transmitting a small-amplitude acoustic pulse will be used. Because of this assumption, it is then valid to use a linear wave equation to describe the propagation of a pulse between source and receiver in an ocean waveguide. Since a linear wave equation is used, it is then valid to treat the ocean as a linear filter. More specifically, it will be treated as a linear, time-invariant, space-variant (LTISV) filter.

The three filter functions discussed in this thesis - the complex frequency response, impulse response, and transfer function - describe the simple waveguide model of the ocean, illustrated in Figure 2.1, where $\rho_1 c_1$, $\rho_2 c_2$, and $\rho_3 c_3$ are the characteristic impedances of media I (air), II (seawater), and III (ocean bottom), respectively. The parameters ρ_i and c_i, $i = 1, 2, 3,$ are the constant ambient (equilibrium) densities (in kilograms per cubic meter) and speeds of sound (in meters per second) in each of the three fluid media, respectively. Both the ocean surface and ocean bottom are modeled as plane, parallel boundaries, and the ocean is D meters deep. The source distribution is a *motionless, time-harmonic, point source* located in medium II at a horizontal range $r = 0$ meters and depth $y = y_0$ meters where the cylindrical coordinates (r, ϕ, y) are illustrated in Figure 2.2.

B. THE COMPLEX FREQUENCY RESPONSE OF THE OCEAN

For an ideal pressure-release surface, ideal rigid bottom ocean waveguide model, the time-invariant, space-variant (TISV) complex frequency response of the ocean is given as follows [6]:

$$\begin{aligned} H_M(f, \mathbf{r} \mid \mathbf{r}_0) &= H_M(f, r, \phi, y \mid y_0) \\ &= -j \frac{1}{2D} \sum_{n=0}^{N_p - 1} \sin(k_{Y_{2,n}} y_0) H_0^{(2)}(k_{r_{2,n}} r) \sin(k_{Y_{2,n}} y), \quad 0 \le y \le D, \end{aligned} \tag{2.1}$$

where

$$N_P = \mathrm{INT}\left(\frac{1}{2}\left[\frac{4Df}{c_2} - 1\right]\right) + 1 \tag{2.2}$$

is the total number of propagating modes excited by the source with frequency f hertz, $H_0^{(2)}(\bullet)$ is the zeroth-order Hankel function of the second kind,

$$k_{r_{2,n}} = \begin{cases} k_2\sqrt{1-(f_n/f)^2}, & f \geq f_n, \\ -jk_2\sqrt{(f_n/f)^2 - 1}, & f < f_n, \end{cases} \tag{2.3}$$

is the propagation-vector component in the horizontal radial direction, in radians per meter, of the *n*th normal mode,

$$k_2 = 2\pi f / c_2 = 2\pi / \lambda_2 \tag{2.4}$$

is the wavenumber in medium II in radians per meter,

$$f_n = \frac{(2n+1)c_2}{4D} \tag{2.5}$$

is the cutoff frequency in hertz of the *n*th normal mode, and

$$k_{Y_{2,n}} = \frac{(2n+1)\pi}{2D} \tag{2.6}$$

represents the propagation-vector component in the depth direction, in radians per meter, of the *n*th normal mode. In the far-field, that is, when $k_{r_{2,n}} r \gg 1$,

$$H_0^{(2)}(k_{r_{2,n}} r) \approx \sqrt{\frac{2}{\pi k_{r_{2,n}} r}} \exp\left[-j\left(k_{r_{2,n}} r - \frac{\pi}{4}\right)\right], \quad k_{r_{2,n}} r \gg 1. \tag{2.7}$$

There are several important things to note. First, the complex frequency response given by equation (2.1) depends on the actual value of the source depth (y_0) and the receiver depth (y) and not the difference between the two. This is an indication that the ocean medium is *space-variant* in the depth direction. Moreover, the number of propagating modes N_p given by (2.2), the cutoff frequency f_n for each mode given by (2.5), and the propagation vector component in the depth direction $k_{Y_{2,n}}$ given by (2.6) all

depend on ocean depth D. Also, (2.1) is the complex frequency response for one frequency. The complex frequency response over a specified range of frequencies from 0 to $f_{\max}$ hertz can be obtained by evaluating (2.1) for each frequency in the range 0 to $f_{\max}$ hertz.

C. THE IMPULSE RESPONSE OF THE OCEAN

The time-invariant, space-variant (TISV) complex frequency response is related to the TISV impulse response by the following equation [6]:

$$H_M(f,\mathbf{r}\,|\,\mathbf{r}_0) = F_\tau\left\{h_M(\tau,\mathbf{r}\,|\,\mathbf{r}_0)\right\} = \int_{-\infty}^{\infty} h_M(\tau,\mathbf{r}\,|\,\mathbf{r}_0)\exp(-j2\pi f\tau)\,d\tau. \tag{2.8}$$

In other words, the complex frequency response is the Fourier transform of the impulse response with respect to the time difference τ. The impulse response is therefore given by

$$h_M(\tau,\mathbf{r}\,|\,\mathbf{r}_0) = F_f^{-1}\left\{H_M(f,\mathbf{r}\,|\,\mathbf{r}_0)\right\} = \int_{-\infty}^{\infty} H_M(f,\mathbf{r}\,|\,\mathbf{r}_0)\exp(+j2\pi f\tau)\,df, \tag{2.9}$$

that is, it is the inverse Fourier transform of the complex frequency response with respect to frequency f. Since (2.9) is an inverse Fourier transform, the impulse response can be numerically evaluated by computing the inverse Discrete Fourier Transform (IDFT) of the complex frequency response as follows:

$$h_M(l) = \frac{1}{L}\sum_{q=0}^{L-1} H_M(q)W_L^{ql}, \quad l = 0,1,...,L-1, \tag{2.10}$$

where $W_L = \exp(+j2\pi/L)$. Note that the total number of time samples L of the impulse response is equal to the total number of frequency samples Q of the complex frequency response (i.e., $L = Q$). The relationship between the DFT bin spacing Δf in hertz, the data record length T in seconds , the number of data points L, and the sampling frequency f_s in hertz is given by

$$\Delta f = \frac{1}{T} = \frac{1}{QT_s} = \frac{f_s}{Q}. \tag{2.11}$$

As can be seen from (2.11), the data record length T of the impulse response determines the spacing Δf between frequency samples of the complex frequency response, that is,

$$\Delta f = \frac{1}{T}. \tag{2.12}$$

The duration of the impulse response T is the *maximum travel time* of the highest propagating mode in the frequency range 0 to $f_{\max}$ hertz with a frequency spacing of 1 hertz.

The maximum travel time, T, is actually an estimate, and is best calculated by computing the *travel time*, $\tau_{r_{2,n}}$, of the highest propagating mode $n = N_p - 1$ for each frequency in the range 0 to $f_{\max}$ hertz and then plotting it versus frequency, as shown in Fig. 2.3. The maximum travel time will then become evident. The travel time of the nth propagating mode at a horizontal range of r meters from the source is given by [7]

$$\tau_{r_{2,n}} = r / c_{g_{r2,n}} \tag{2.13}$$

where the *group speed* is given by

$$c_{g_{r2,n}} = c_2 \sqrt{1-(f_n / f)^2}, \quad f \geq f_n, \quad n = N_p - 1. \tag{2.14}$$

The maximum travel time T is then given by

$$T = \max \tau_{r_{2,n}} \; \forall f = 0,1,2,....,f_{\max}, \quad n = N_p - 1. \tag{2.15}$$

Once T is computed or obtained visually from a plot, Δf can then be computed from (2.12).

The total number of frequency samples Q to be taken of the complex frequency response was computed from the following equation:

$$Q = 2\frac{f_{\max}}{\Delta f} + 1 \tag{2.16}$$

where Δf is given by (2.12) and $f_{\max}$ is the maximum frequency component in hertz used to evaluate the complex frequency response. Note that Q computed from (2.16) will be an odd number. Once the value of Q is determined, it can be used to compute the sampling period T_s in seconds from [see (2.11)]

$$T_s = \frac{1}{Q\Delta f} \tag{2.17}$$

The time samples of the impulse response correspond to time instants

$$\tau = lT_s, \quad l = 0,1,...,L-1, \tag{2.18}$$

where $L = Q$.

In order to evaluate (2.10), we took advantage of the conjugate symmetry property of the complex frequency response, which is

$$H_M(-f, \mathbf{r} \mid \mathbf{r}_0) = H_M^*(f, \mathbf{r} \mid \mathbf{r}_0). \tag{2.19}$$

Therefore, since Q is odd, the following equation was used to generate values for $H_M(q)$ in (2.10) for $q = Q' + 1, Q' + 2, ..., Q - 1$ where $Q' = (Q-1)/2$:

$$H_M(q) = H_M^*(Q-q), \quad q = Q' + 1, Q' + 2, ..., Q - 1. \tag{2.20}$$

Finally, we are able to compute the inverse Discrete Fourier Transform (IDFT) of the complex frequency response to generate the impulse response:

$$h_M(l, \mathbf{r} \mid \mathbf{r}_0) = IDFT\{H_M(q, \mathbf{r} \mid \mathbf{r}_0)\} = \frac{1}{Q}\sum_{q=0}^{Q-1} H_M(q, \mathbf{r} \mid \mathbf{r}_0) W_q^{ql}, l = 0,1,...,L-1 \tag{2.21}$$

D. THE TRANSFER FUNCTION OF THE OCEAN

Given a time-invariant, space-variant complex frequency response, it is possible to derive the corresponding *time-invariant, space-variant, transfer function* of the ocean by using the following general expression[6]:

$$\underline{H}_M(f, \mathbf{r} \mid \mathbf{v}) = \int_{-\infty}^{\infty} H_M(f, \mathbf{r} \mid \mathbf{r}_0) \exp\left[+j2\pi \mathbf{v} \bullet (\mathbf{r} - \mathbf{r}_0)\right] d\mathbf{r}_0 \tag{2.22}$$

where f represents the transmitted frequencies in hertz, $\mathbf{v} = (f_X, f_Y, f_Z)$ is a three-dimensional vector whose components are transmitted spatial frequencies in cycles per meter in the *X*, *Y*, and *Z* directions, respectively, and $d\mathbf{r}_0 = dx_0 dy_0 dz_0$.

The spatial frequencies $f_X, f_Y,$ and f_Z are given by

$$f_X = \frac{u_0}{\lambda_0}, \tag{2.23}$$

$$f_Y = \frac{v_0}{\lambda_0}, \tag{2.24}$$

$$f_Z = \frac{w_0}{\lambda_0}, \tag{2.25}$$

where

$$u_0 = \sin\theta_0 \cos\psi_0, \tag{2.26}$$

$$v_0 = \sin\theta_0 \sin\psi_0, \tag{2.27}$$

$$w_0 = \cos\theta_0 \tag{2.28}$$

are *dimensionless direction cosines* with respect to the *X*, *Y*, and *Z* axes, respectively, θ_0 and ψ_0 are spherical angles that describe the directions of wave propagation at the transmitter. In these expressions,

$$c_0 = f\lambda_0, \tag{2.29}$$

where c_0 is the speed of sound in meters per second in the waveguide, f represents the transmitted frequencies in hertz, and λ_0 is the corresponding wavelength in meters. Therefore, the transmitted spatial frequencies describe the directions of wave propagation at the transmitter.

From (2.22), we can write that

$$\underline{H}_M(f, \mathbf{r} \mid f_X, f_Y, f_Z) = \int_{-\infty}^{\infty}\int_{-\infty}^{\infty}\int_{-\infty}^{\infty} H_M(f, \mathbf{r} \mid x_0, y_0, z_0) \times \exp\{+j2\pi[f_X(x-x_0) + f_Y(y-y_0) + f_Z(z-z_0)]\}\, dx_0 dy_0 dz_0. \tag{2.30}$$

Since the complex frequency response given by (2.1) depends only on the depths of the source and receiver, we will concentrate on trying to evaluate the following single integral:

$$\underline{H}_M\left(f,\mathbf{r}\,|\,x_0,f_Y,z_0\right)=\int_{-\infty}^{\infty}H_M\left(f,\mathbf{r}\,|\,x_0,y_0,z_0\right)\exp\left\{+j2\pi\left[f_Y(y-y_0)\right]\right\}dy_0. \tag{2.31}$$

Equation (2.26) can be rewritten as

$$\underline{H}_M\left(f,\mathbf{r}\,|\,x_0,f_Y,z_0\right)=\int_{-\infty}^{\infty}H_M\left(f,\mathbf{r}\,|\,x_0,y_0,z_0\right)\exp\left(-j2\pi f_Y y_0\right)dy_0\exp(+j2\pi f_Y y) \tag{2.32}$$

or

$$\underline{H}_M\left(f,r,\phi,y\,|\,f_Y\right)=\int_{-\infty}^{\infty}H_M\left(f,r,\phi,y\,|\,y_0\right)\exp\left(-j2\pi f_Y y_0\right)dy_0\exp(+j2\pi f_Y y) \tag{2.33}$$

since from (2.1),

$$H_M(f,\mathbf{r}\,|\,\mathbf{r}_0)=H_M(f,r,\phi,y\,|\,y_0)=-j\frac{1}{2D}\sum_{n=0}^{N_p-1}\sin(k_{Y_{2,n}}y_0)H_0^{(2)}(k_{r_{2,n}}r)\sin(k_{Y_{2,n}}y),\ 0\le y\le D. \tag{2.34}$$

Substituting (2.34) into (2.33) yields

$$\underline{H}_M\left(f,r,\phi,y\,|\,f_Y\right)=\int_{-\infty}^{\infty}-j\frac{1}{2D}\sum_{n=0}^{N_p-1}\sin(k_{Y_{2,n}}y_0)H_0^{(2)}(k_{r_{2,n}}r)\sin(k_{Y_{2,n}}y)\exp\left(-j2\pi f_Y y_0\right)dy_0\times \exp(+j2\pi f_Y y),\ 0\le y\le D. \tag{2.35}$$

Since the integration is only with respect to y_0, (2.30) becomes

$$\underline{H}_M\left(f,r,\phi,y\,|\,f_Y\right)=-j\frac{1}{2D}\sum_{n=0}^{N_p-1}H_0^{(2)}(k_{r_{2,n}}r)\sin(k_{Y_{2,n}}y)\int_{-\infty}^{\infty}\sin(k_{Y_{2,n}}y_0)\exp\left(-j2\pi f_Y y_0\right)dy_0\times \exp(+j2\pi f_Y y),\ 0\le y\le D. \tag{2.36}$$

Also, since the depth of the source $0\le y_0\le D$, and if we let

$$k_{Y_{2,n}}=2\pi f_{Y_{2,n}}, \tag{2.37}$$

then the integral in (2.36) is given by

$$\int_0^D \sin\left(2\pi f_{Y_{2,n}} y_0\right)\exp\left(-j2\pi f_Y y_0\right)dy_0 =$$
$$\frac{D}{2}\{\exp\left(-j\pi/2\right)\mathrm{sinc}[(f_Y - f_{Y_{2,n}})D]\exp[-j\pi(f_Y - f_{Y_{2,n}})D] + \qquad (2.38)$$
$$\exp(+j\pi/2)\,\mathrm{sinc}[(f_Y + f_{Y_{2,n}})D]\exp[-j\pi(f_Y + f_{Y_{2,n}})D]\}$$

In the above equations [see (2.19), (2.22), and (2.24)]

$$f_Y = \frac{v_0}{\lambda_0} = \frac{f}{c_0}\cos\beta_0, \quad 0 \le \beta_0 \le 90^\circ, \qquad (2.39)$$

since direction cosine v_0 is also equal to $\cos\beta_0$ where β_0 is measured from the positive Y axis. Note that although β_0 can be between 0 and 180°, the angles of propagation of the normal modes in the waveguide are restricted between 0 and 90°. Substituting (2.38) into (2.36), we have

$$\underline{H}_M\left(f, r, \phi, y \mid f_Y\right) = -j\frac{1}{4}\sum_{n=0}^{N_p-1} H_0^{(2)}(k_{r_{2,n}} r)\sin(k_{Y_{2,n}} y)\times$$
$$\{\exp(-j\pi/2)\mathrm{sinc}[(f_Y - f_{Y_{2,n}})D]\exp[-j\pi(f_Y - f_{Y_{2,n}})D] \qquad (2.40)$$
$$+\exp(+j\pi/2)\,\mathrm{sinc}[(f_Y + f_{Y_{2,n}})D]\exp[-j\pi(f_Y + f_{Y_{2,n}})D]\}\exp(+j2\pi f_Y y),$$

which is the transfer function of the ocean with respect to depth. It is important to note that the transfer function depends on the angle β_0 via (2.34). Therefore, (2.35) can be computed numerically by summing the response of each mode at a given frequency and angle β_0. Thus, a response over $0 \le \beta_0 \le 90^\circ$ can be obtained.

E. SUMMARY

By modeling the ocean as a linear, time-invariant, space-variant filter, three filter functions were obtained. These functions are the complex frequency response, the impulse response, and the transfer function of the ocean. The complex frequency response can be discretized and then related to the impulse response through the use of an inverse discrete Fourier transform. The impulse response is a time-domain expression that yields useful information regarding the location of the sound source. Lastly, a closed form expression for the transfer function of the ocean with respect to depth was obtained

from the complex frequency response. The transfer function can be used to investigate the behavior of the ocean as a function of the angle of propagation of sound leaving the sound source.

THIS PAGE INTENTIONALLY LEFT BLANK

III. COMPUTER SIMULATION RESULTS AND ANALYSIS

A. OVERVIEW

This chapter presents computer simulation results obtained by evaluating the following equations from Chapter II: the time – invariant, space – variant (TISV) complex frequency response of the ocean given by (2.1), the TISV impulse response given by (2.21), and the TISV transfer function with respect to depth given by (2.40). These three ocean-medium filter functions were evaluated for the test cases shown in Table 3.1.

	A	B	C	D	E
1	$r = 300$ m $y_0 = 5$ m $y = 5$ m $\Delta y = 0$ m	$r = 300$ m $y_0 = 50$ m $y = 50$ m $\Delta y = 0$ m	$r = 300$ m $y_0 = 95$ m $y = 95$ m $\Delta y = 0$ m	$r = 300$ m $y_0 = 50$ m $y = 5$ m $\Delta y = -45$ m	$r = 300$ m $y_0 = 50$ m $y = 95$ m $\Delta y = 45$ m
2	$r = 500$ m $y_0 = 5$ m $y = 5$ m $\Delta y = 0$ m	$r = 500$ m $y_0 = 50$ m $y = 50$ m $\Delta y = 0$ m	$r = 500$ m $y_0 = 95$ m $y = 95$ m $\Delta y = 0$ m	$r = 500$ m $y_0 = 50$ m $y = 5$ m $\Delta y = -45$ m	$r = 500$ m $y_0 = 50$ m $y = 95$ m $\Delta y = 45$ m
3	$r = 1000$ m $y_0 = 5$ m $y = 5$ m $\Delta y = 0$ m	$r = 1000$ m $y_0 = 50$ m $y = 50$ m $\Delta y = 0$ m	$r = 1000$ m $y_0 = 95$ m $y = 95$ m $\Delta y = 0$ m	$r = 1000$ m $y_0 = 50$ m $y = 5$ m $\Delta y = -45$ m	$r = 1000$ m $y_0 = 50$ m $y = 95$ m $\Delta y = 45$ m

Table 3.1. Test Cases

In this table, r is the horizontal range between source and receiver, y_0 is the depth of the source, y is the depth of the receiver, and $\Delta y = y - y_0$ is the depth offset between source and receiver. These computer simulation results will show that an impulse response contains information on the range and depth separation between a receiver and a target.

Unless indicated otherwise, it is important to note that a Δf of 0.1 Hz was used to generate the computer simulation results. This corresponds to a maximum travel time T of 10 seconds. This was done to allow as many propagating modes as possible to be

included in the complex frequency response, and therefore in the impulse response, while still allowing the simulation to run within a reasonable time. Allowing for a longer travel time greatly reduces the spikes that appear prior to $\tau_{\min}$, which is the minimum possible travel time between source and receiver for a given range separation r, or simply r/c, where c is the sound speed in the waveguide. These spikes are artifacts created by the computer simulation due to Δf being too large. Figure 3.1 illustrates the modal travel times for the highest – order propagating modes for a horizontal range of $r = 1000$ meters versus frequency in an ideal pressure – release surface, rigid bottom ocean waveguide. In the following plots for the normalized impulse response, only 1 second worth of data is shown although 10 seconds of data is available. The spikes in front of $\tau_{\min}$ can be explained by the fact that since $\Delta f = 0.1$ Hz, all 30 seconds of data were not included in the impulse response. Figure 3.2 demonstrates that extraneous spikes can be reduced by decreasing Δf which increases T_0.

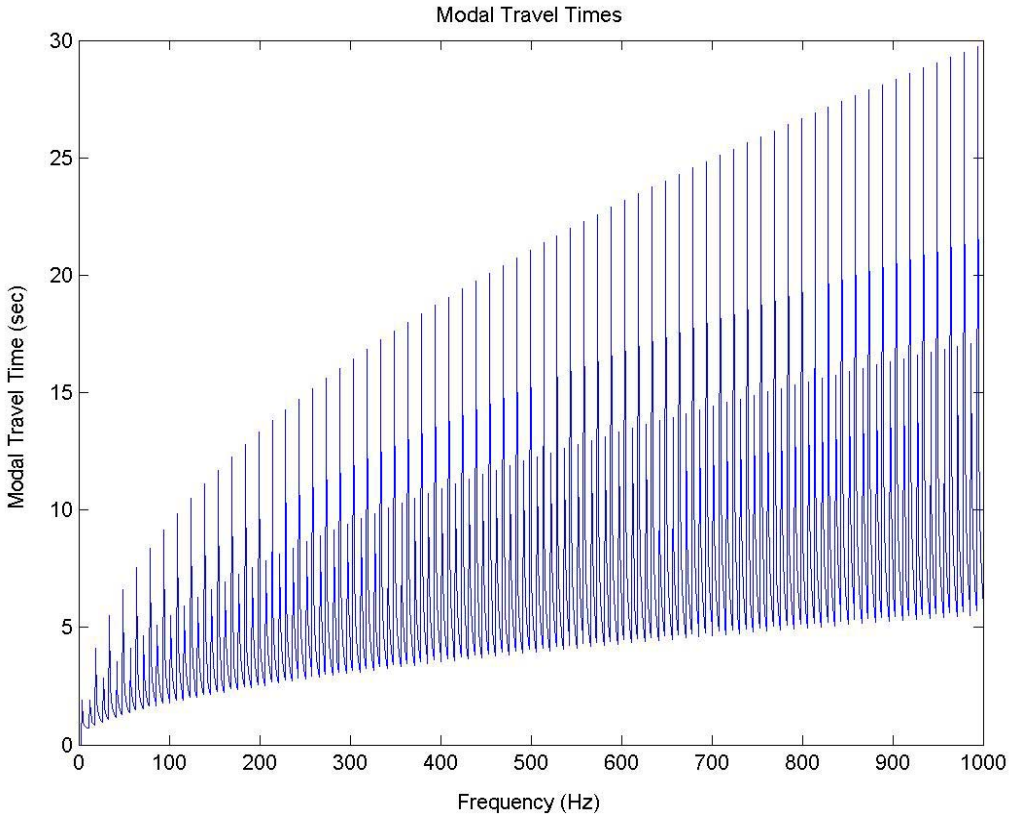

Figure 3.1. Modal travel times for the highest – order propagating mode for a horizontal range r = 1000 m for each transmitted frequency.

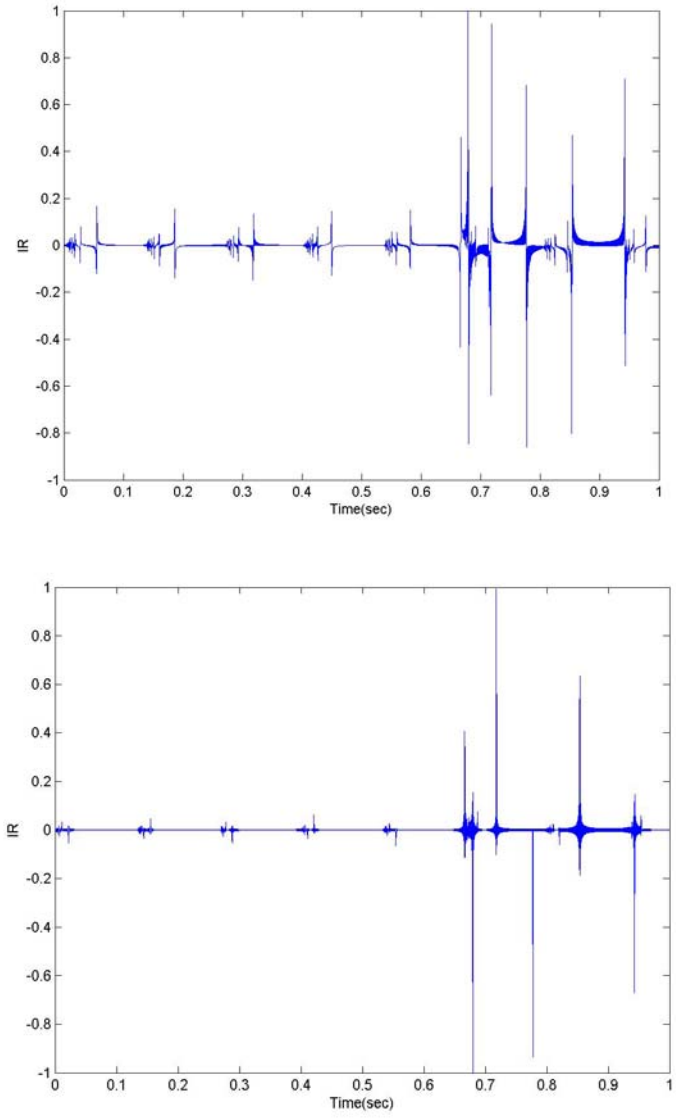

Figure 3.2. Normalized impulse response (IR) for Case 3B, for a Δf of .25 Hz versus a Δf of .1 Hz. Notice how reducing the bin spacing Δf decreases the extraneous spikes.

B. ZERO DEPTH OFFSET

In terms of depth separation, the impulse response given by (2.21) can be used to determine whether the sound source (target) is at the same depth as the receiver. For cases 'A' through 'C' (see Table 3.1), the impulse response (IR) plots are distinguished by alternating positive and negative spikes. The spikes become much more regularly spaced as time elapses. Notice that for each of the nine impulse response plots presented in this section, there is no distinguishable pattern for either the magnitude or phase of the

normalized complex frequency response (CFR). The complex frequency response, for all intents and purposes, looks like noise, especially for cases 'B'.

For each of the cases 'A', the depth offset remained 0 and only the range was altered. Cases 1, 2, and 3 had range separations of 300, 500, and 1000 meters, respectively. Notice that even though 30 seconds of impulse response data should have been included to account for all the modes, the plots have relatively small extraneous spikes. Also important to note is that the travel time τ_1 of the maximum amplitude spike (+1 or –1) in the impulse response always appears just after the minimum travel time $\tau_{\min}$, as shown in Table 3.2. We shall refer to these travel times as the maximum-amplitude travel times.

Case	$\tau_{\min}$ **(sec)**	τ_1 **(sec)**
1A	2.0000e-001	2.4049e-001
2A	3.3333e-001	3.5898e-001
3A	6.6666e-001	7.1796e-001

Table 3.2. Minimum travel times versus maximum – amplitude travel times.

Similar results were achieved for cases 'B' and 'C', where there was no depth offset. The graphs appeared remarkably similar, with subtle differences that would not be relevant to localization in depth.

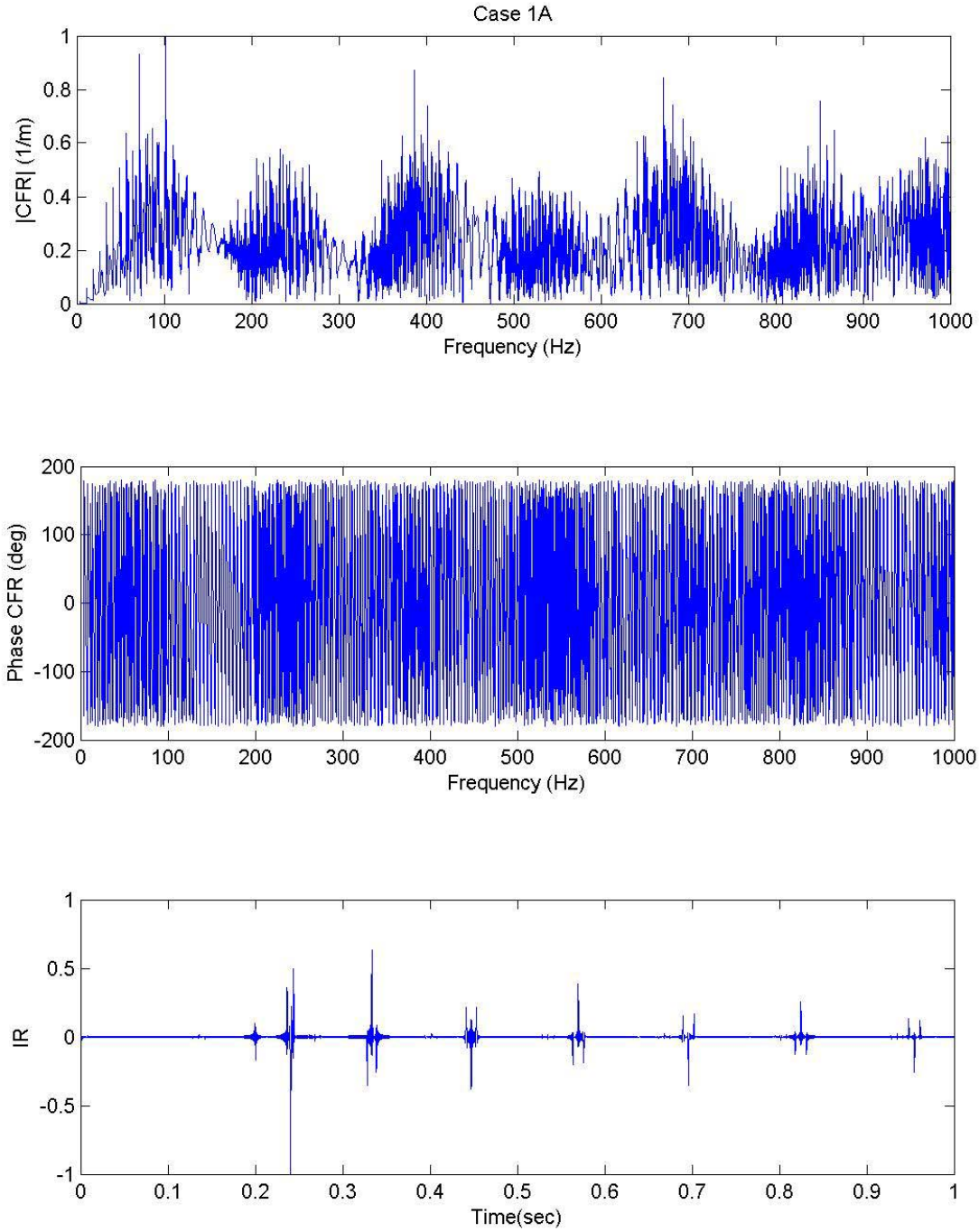

Figure 3.3. Magnitude and phase of complex frequency response (CFR) and impulse response (IR) for Case 1A.

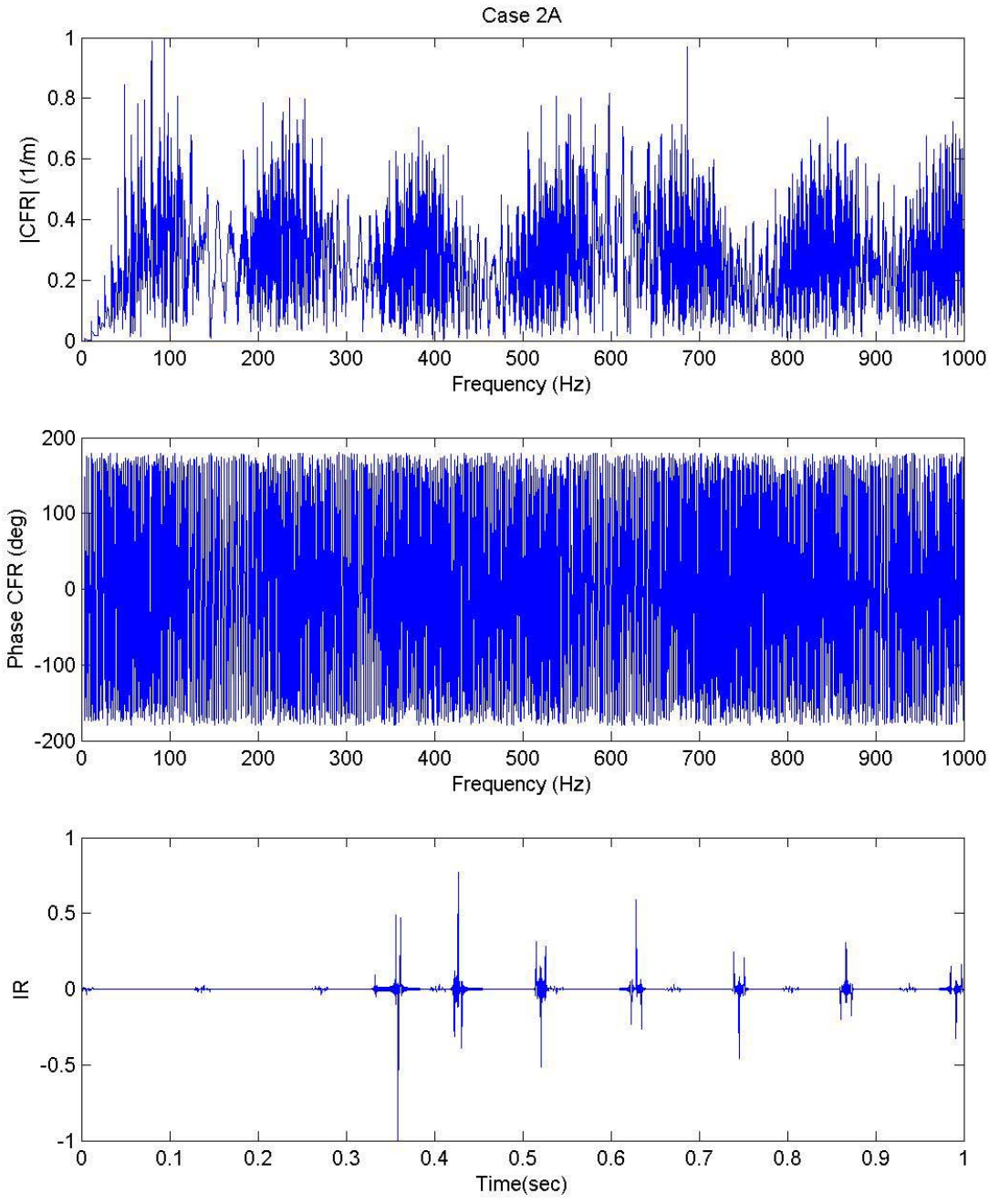

Figure 3.4. Magnitude and phase of complex frequency response (CFR) and impulse response (IR) for Case 2A.

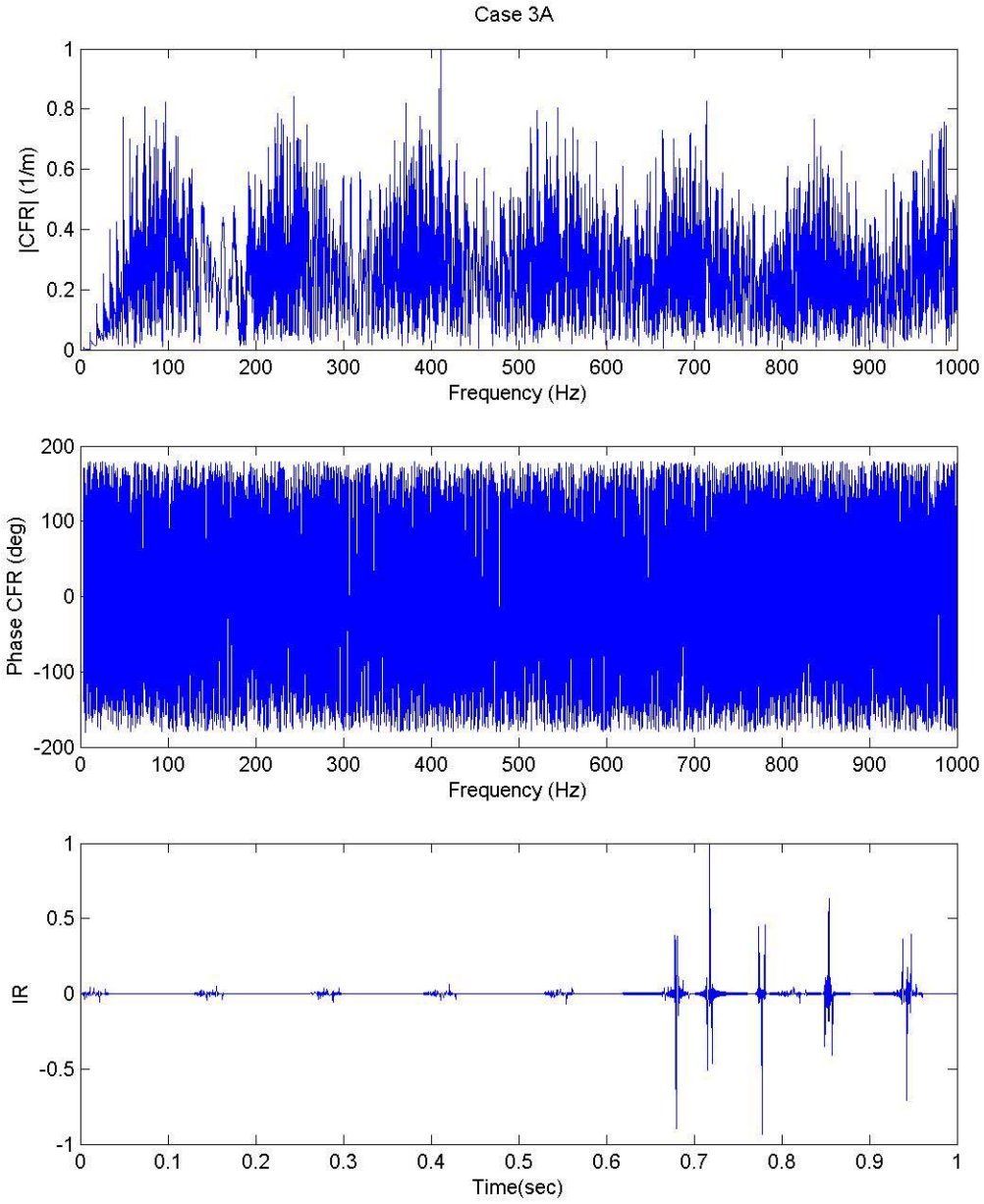

Figure 3.5. Magnitude and phase of complex frequency response (CFR) and impulse response (IR) for Case 3A.

Case	τ_{min} (sec)	τ_1 (sec)
1B	2.0000e-001	2.4049e-001
2B	3.3333e-001	3.5898e-001
3B	6.6667e-001	6.7997e-001

Table 3.3. Minimum travel times versus maximum – amplitude travel times.

A comparison between Tables 3.3 and 3.4 for cases 'B' and 'C' shows the maximum – amplitude spike at different points in time. For case 1C, due to numerical errors, the maximum – amplitude spike actually arrives sooner than is physically possible. The simulation was run again for case 1C, this time allowing 30 seconds worth of data to accumulate. Even though all propagating modes were allowed to come in, the same results were achieved due to machine precision errors. The goal of the tables, however, is to show that the maximum – amplitude travel time can be used to compute a good estimate of the range to the target. In all three tables so far, the simulation was able to provide a maximum bound on the range through timing of the maximum – amplitude spike.

Case	τ_{min} (sec)	τ_1 (sec)
1C	2.0000e-001	1.9999e-001
2C	3.3333e-001	3.5898e-001
3C	6.6667e-001	6.7997e-001

Table 3.4. Minimum travel times versus maximum – amplitude travel times.

Figures 3.6 through 3.11 show graphically the results shown by Tables 3.3 and 3.4. Notice that for each plot of the impulse response, the maximum – amplitude spike arrives shortly after the minimum travel time. Moreover, for each of the cases 'B' and 'C', the impulse response plots show spikes that alternate between positive and negative amplitude values, and show a similar pattern.

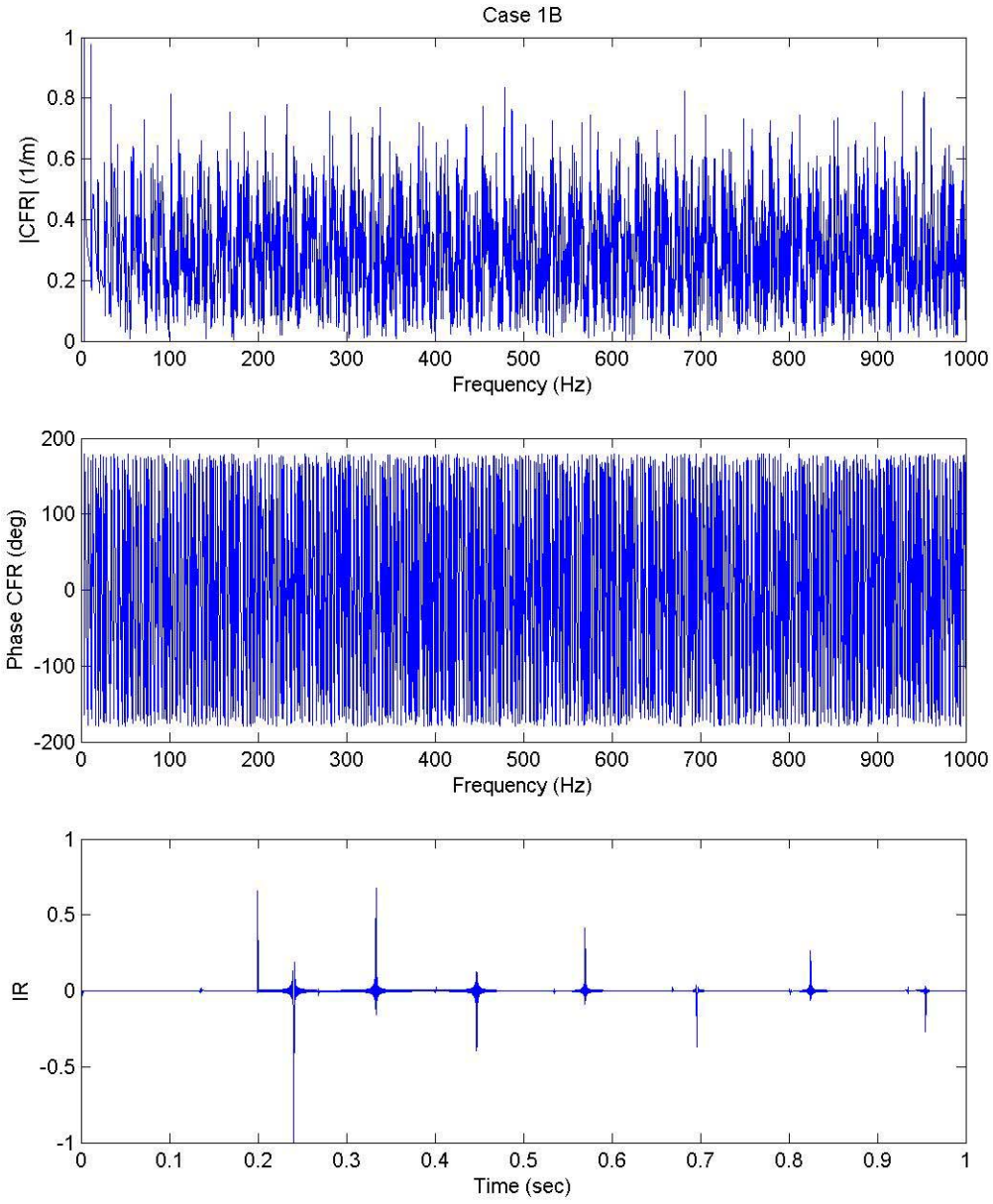

Figure 3.6. Magnitude and phase of complex frequency response (CFR) and impulse response (IR) for Case 1B.

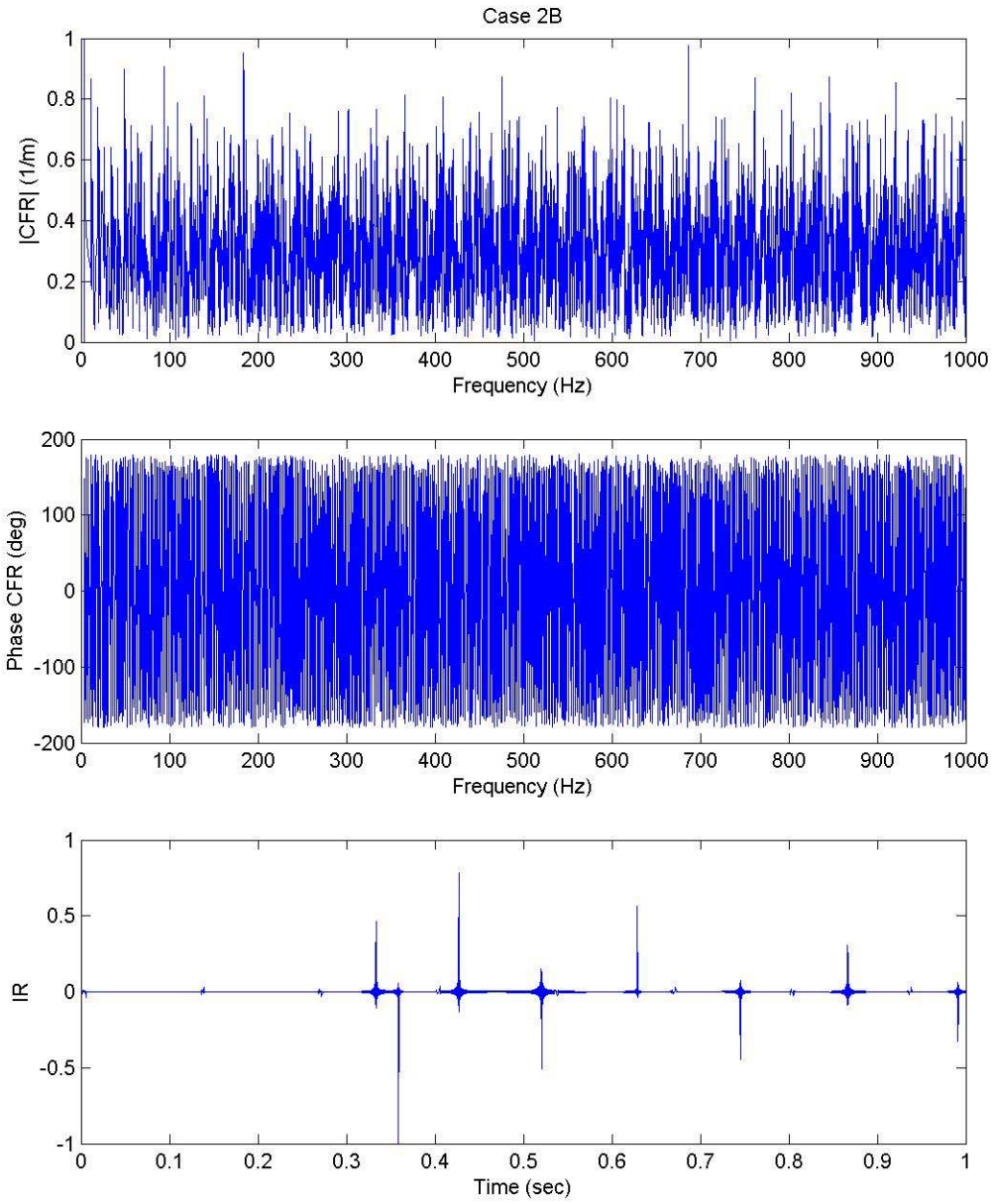

Figure 3.7. Magnitude and phase of complex frequency response (CFR) and impulse response (IR) for Case 2B.

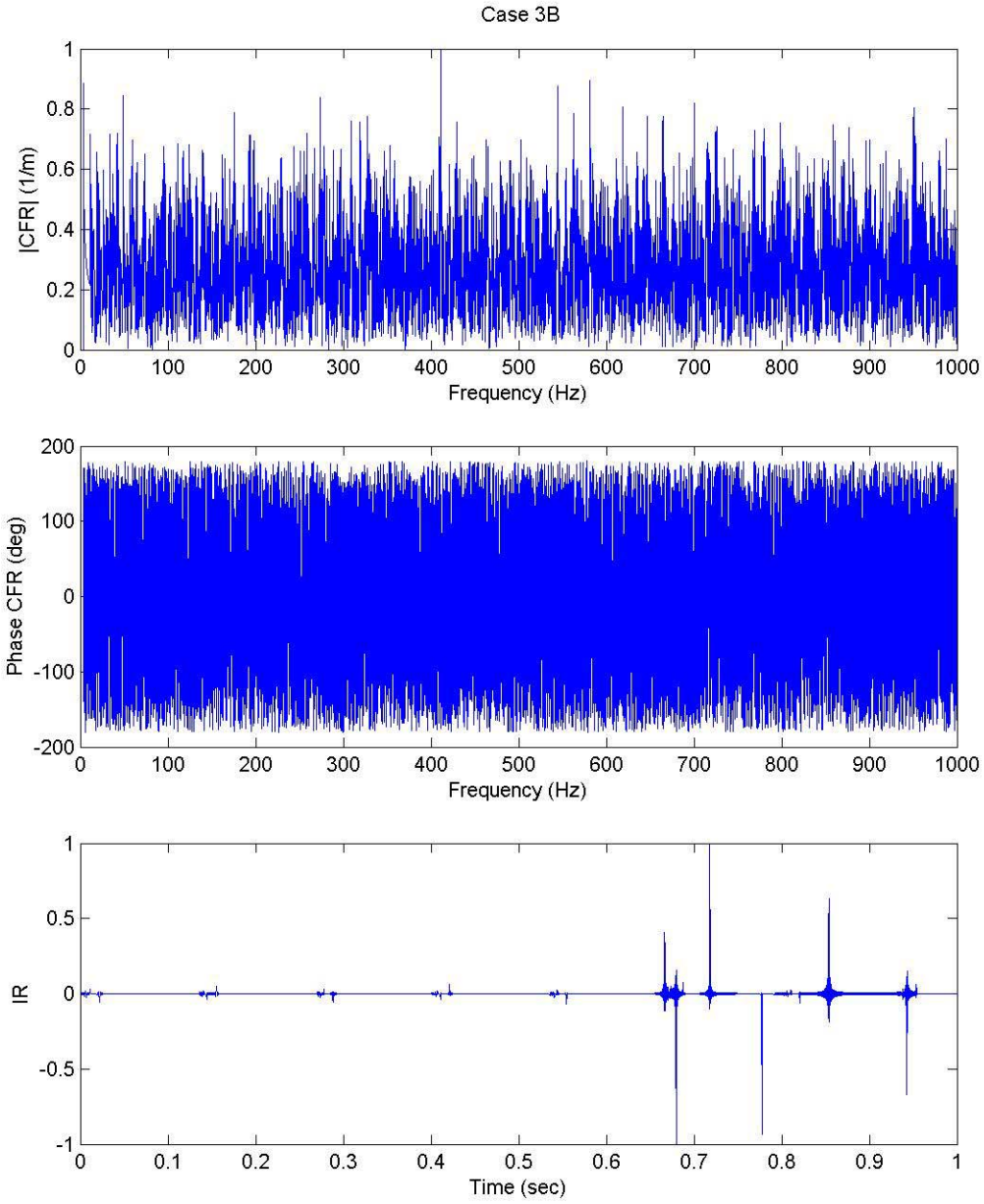

Figure 3.8. Magnitude and phase of complex frequency response (CFR) and impulse response (IR) for Case 3B.

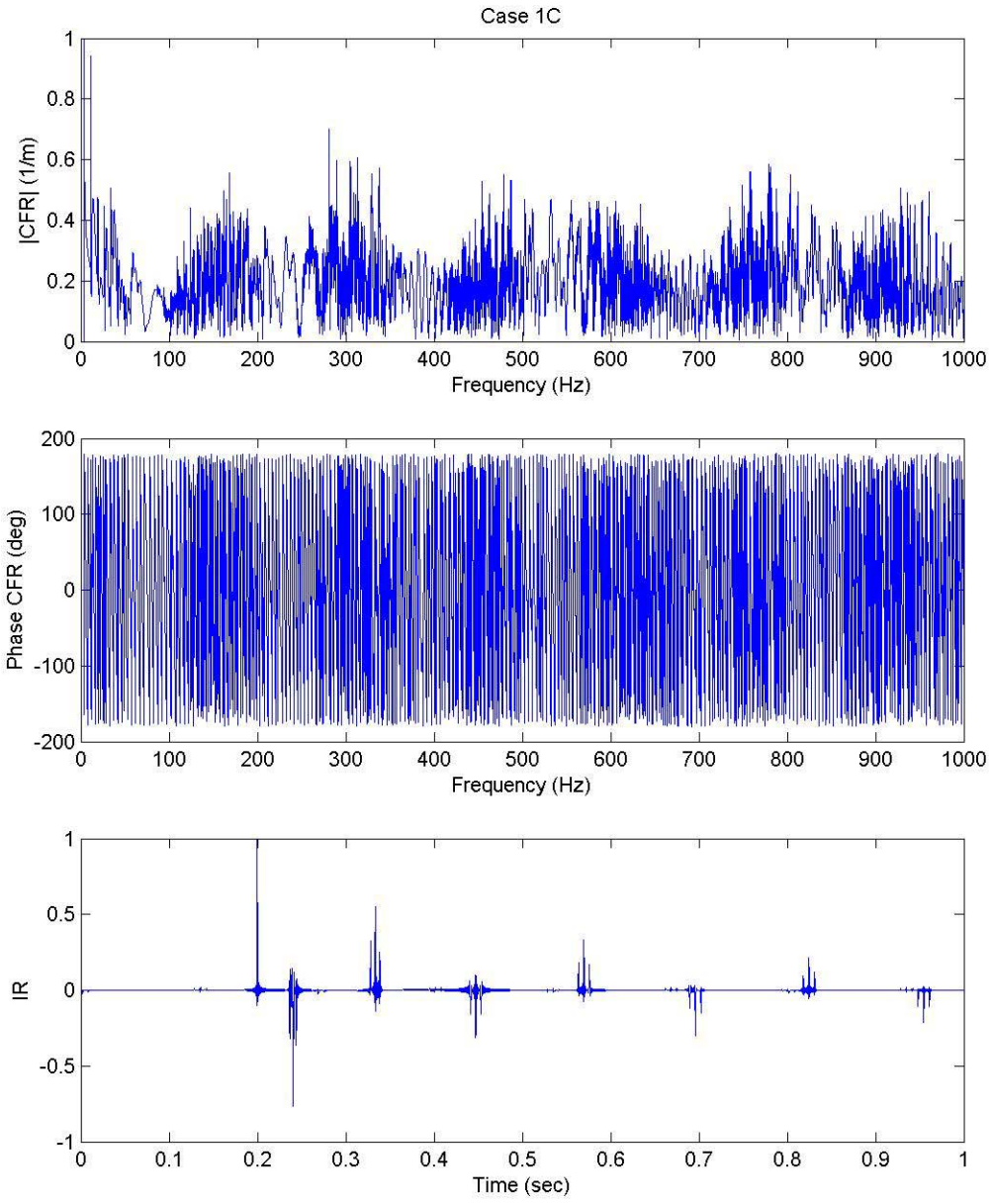

Figure 3.9. Magnitude and phase of complex frequency response (CFR) and impulse response (IR) for Case 1C.

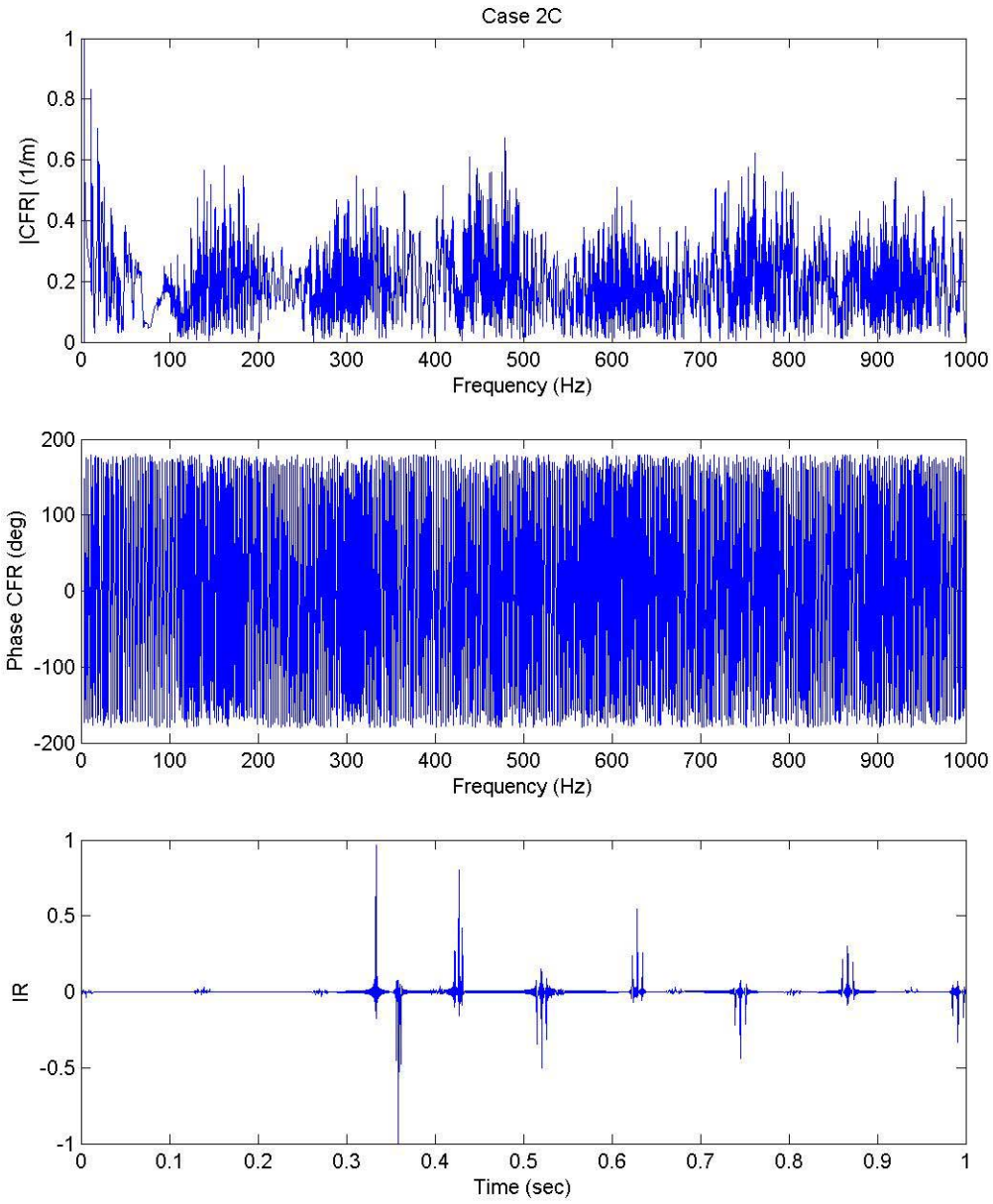

Figure 3.10. Magnitude and phase of complex frequency response (CFR) and impulse response (IR) for Case 2C.

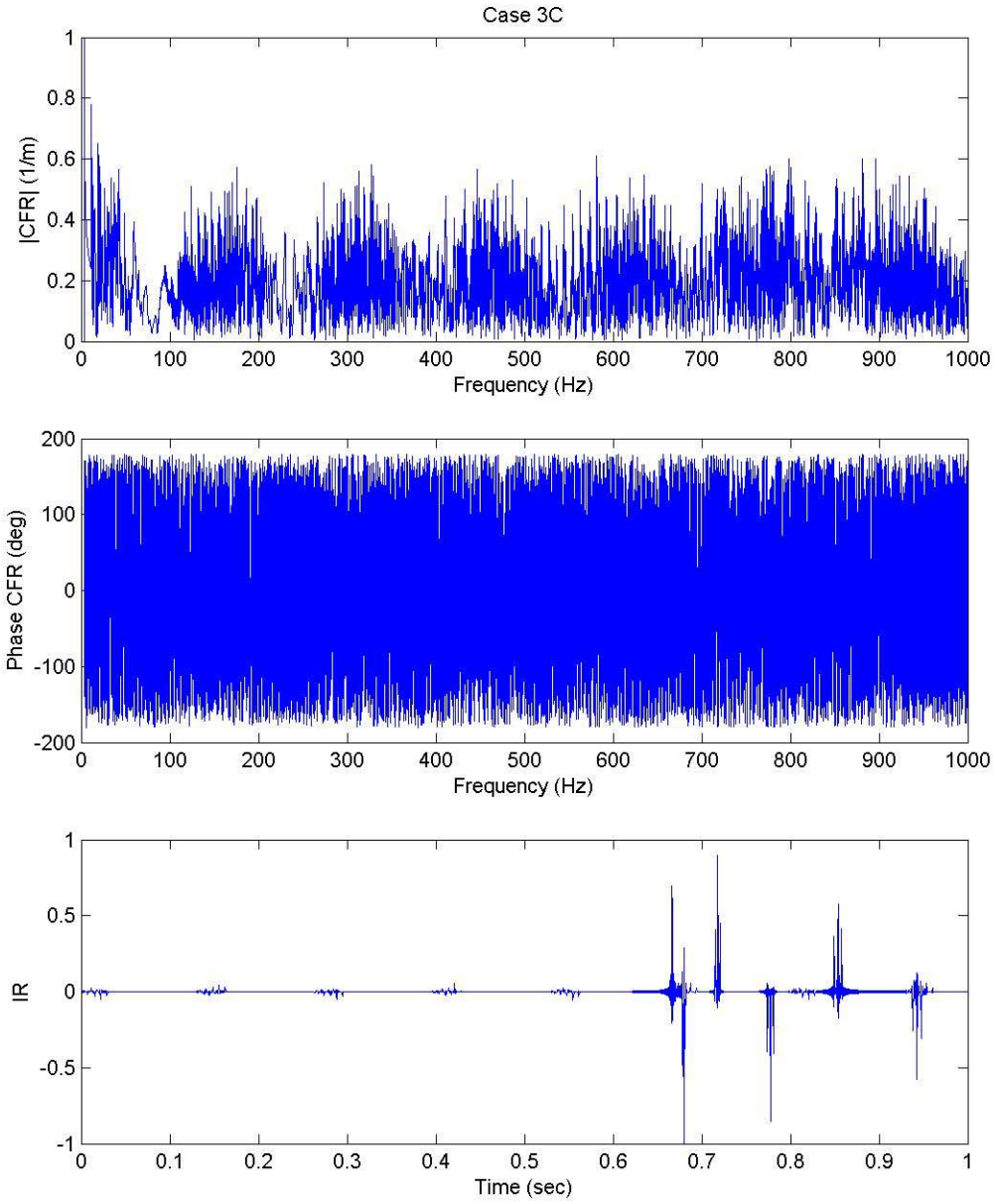

Figure 3.11. Magnitude and phase of complex frequency response (CFR) and impulse response (IR) for Case 3C.

C. NEGATIVE DEPTH OFFSET

Having already shown that a target at the same depth as the receiver can be localized in range, the qualitative nature of a negative depth offset will now also be shown. Table 3.5 shows the minimum travel times versus maximum – amplitude travel times for cases 'D':

Case	$\tau_{\min}$ **(sec)**	τ_1 **(sec)**
1D	2.0000e-001	2.2499e-001
2D	3.3333e-001	3.3548e-001
3D	6.6667e-001	6.8797e-001

Table 3.5. Minimum travel times versus maximum – amplitude travel times.

Just as before, the maximum – amplitude travel time can be used to compute a good estimate of the range to the target. As Figs. 3.12 through 3.14 show, the presence of a negative depth offset can be determined empirically from the impulse response plots. For each impulse response, the spikes are equally positive and negative at each point in time that they appear.

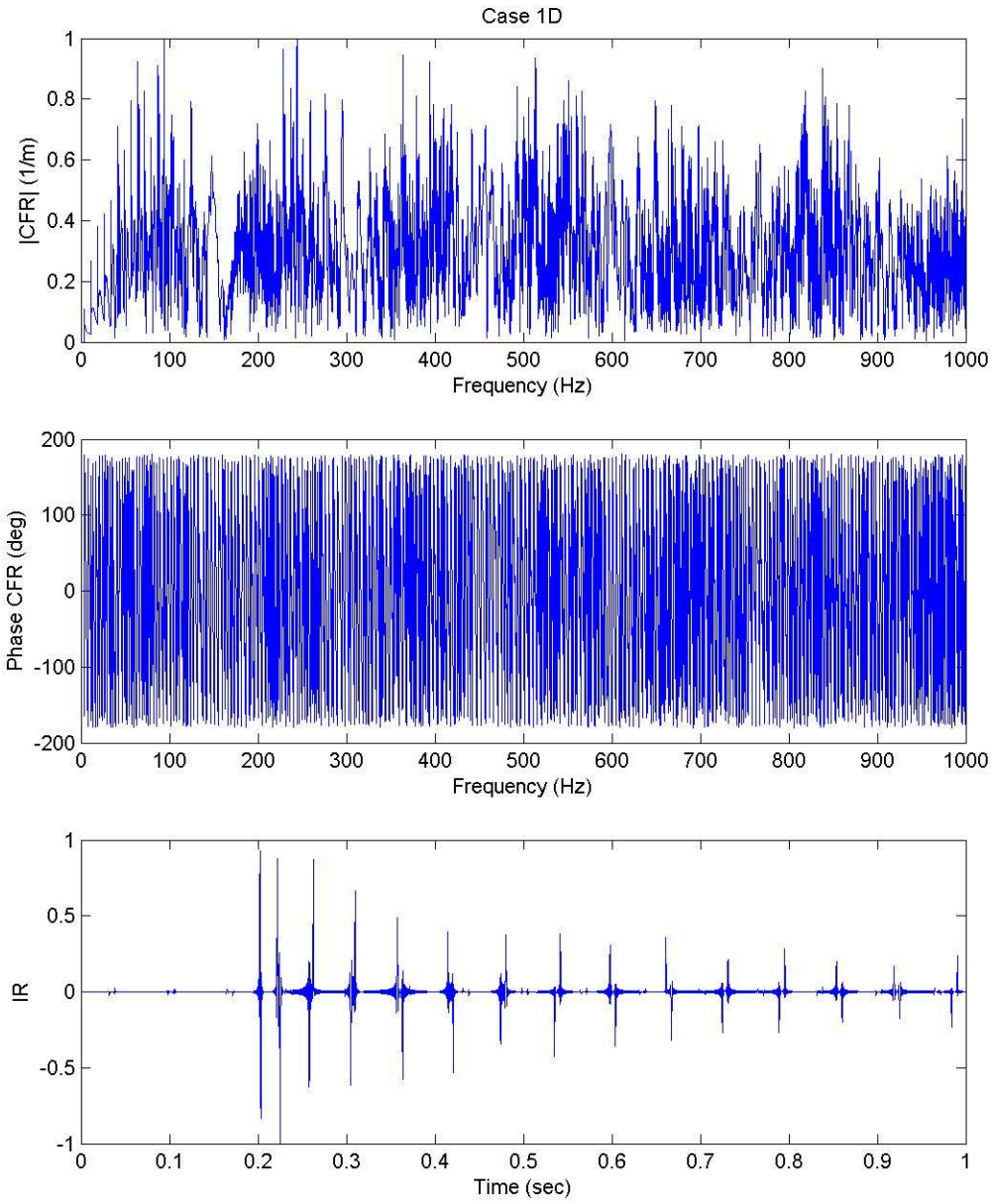

Figure 3.12. Magnitude and phase of complex frequency response (CFR) and impulse response (IR) for Case 1D.

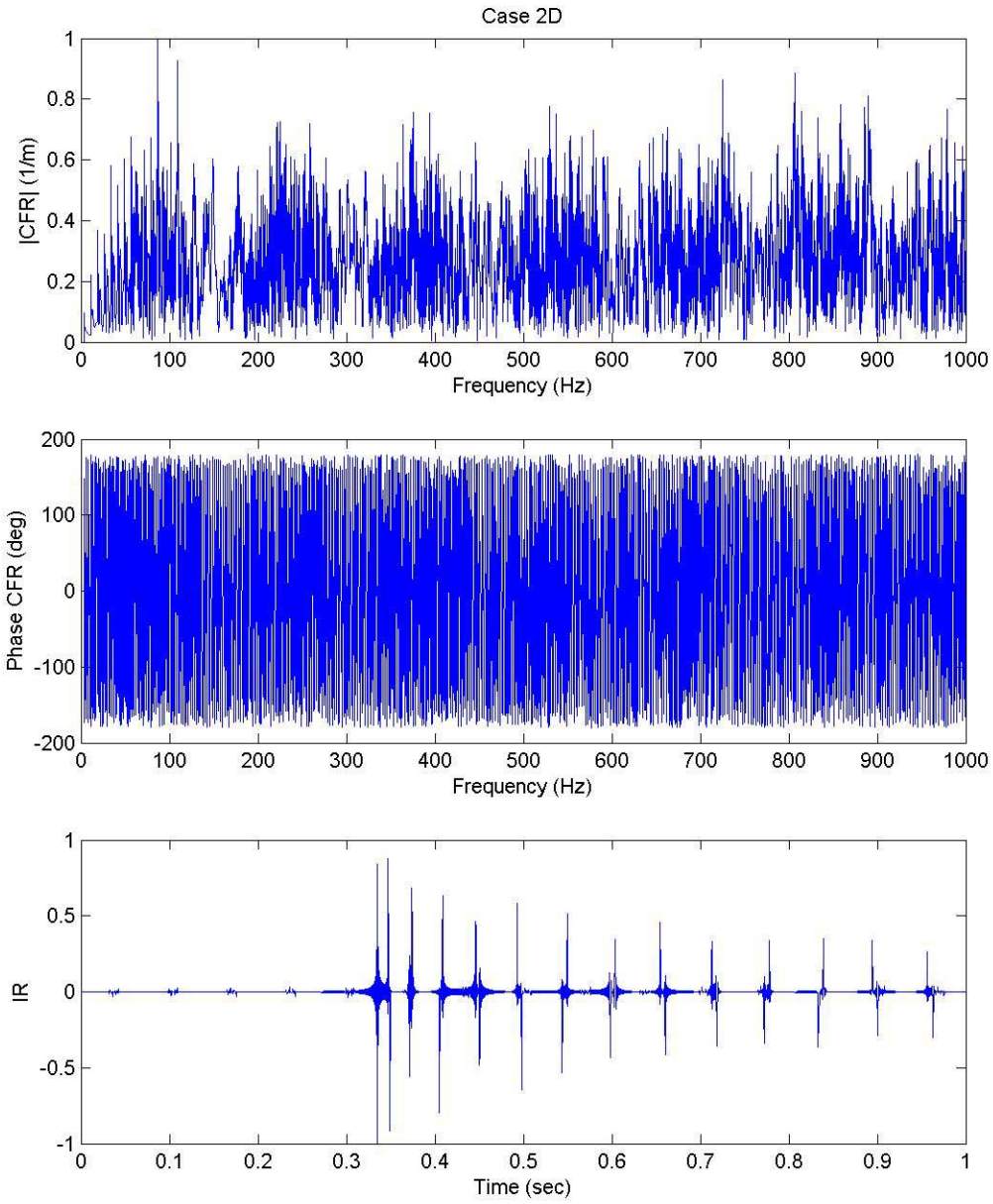

Figure 3.13. Magnitude and phase of complex frequency response (CFR) and impulse response (IR) for Case 2D.

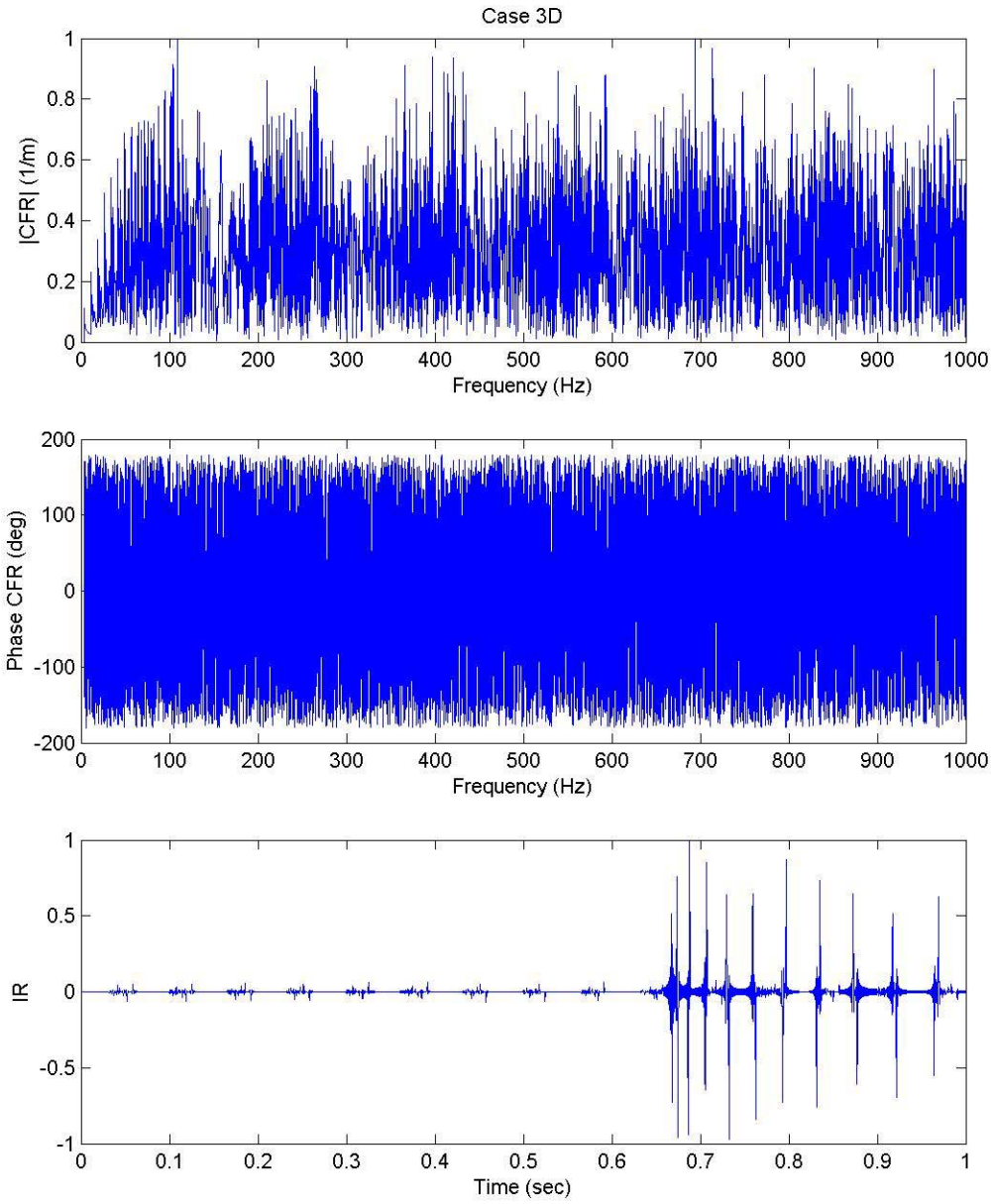

Figure 3.14. Magnitude and phase of complex frequency response (CFR) and impulse response (IR) for Case 3D.

D. POSITIVE DEPTH OFFSET

Just as a negative depth offset has characteristics that manifest themselves in the impulse response plot, a positive depth offset has its own characteristics as well. For each of the cases 'E', (Figures. 3.15 through 3.17), a positive depth offset of 45 meters was used. Note the very distinctive pattern exhibited by the spikes in these figures. Table 3.6 demonstrates the range localization capability of the impulse response for a positive depth offset by showing how the maximum amplitude spikes arrive close to the minimum travel time r/c:

Case	$\tau_{\min}$ **(sec)**	τ_1 **(sec)**
1E	2.0000e-001	2.0349e-001
2E	3.3333e-001	3.3498e-001
3E	6.6667e-001	6.6747e-001

Table 3.6. Minimum travel times versus maximum – amplitude travel times.

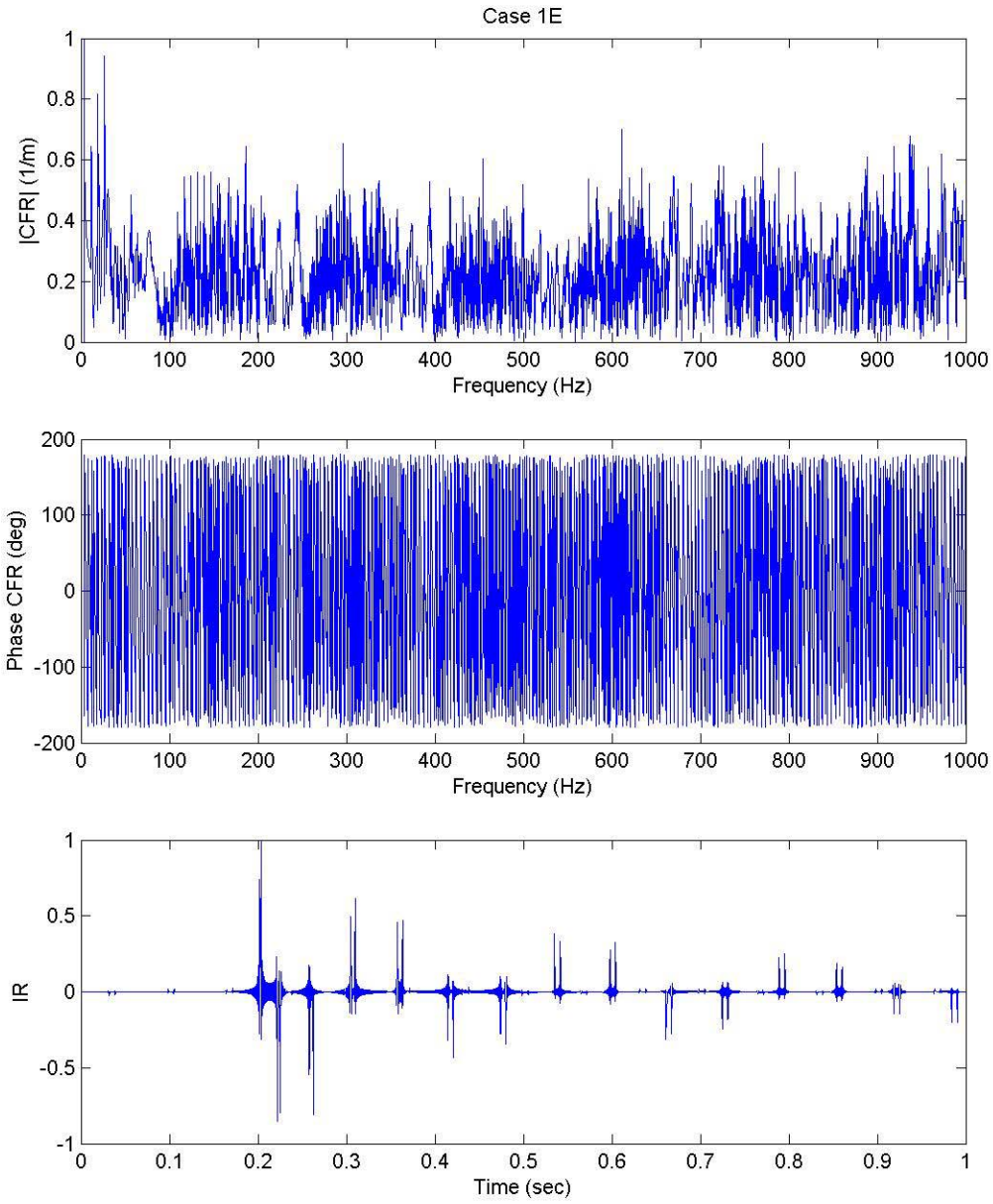

Figure 3.15. Magnitude and phase of complex frequency response (CFR) and impulse response (IR) for Case 1E.

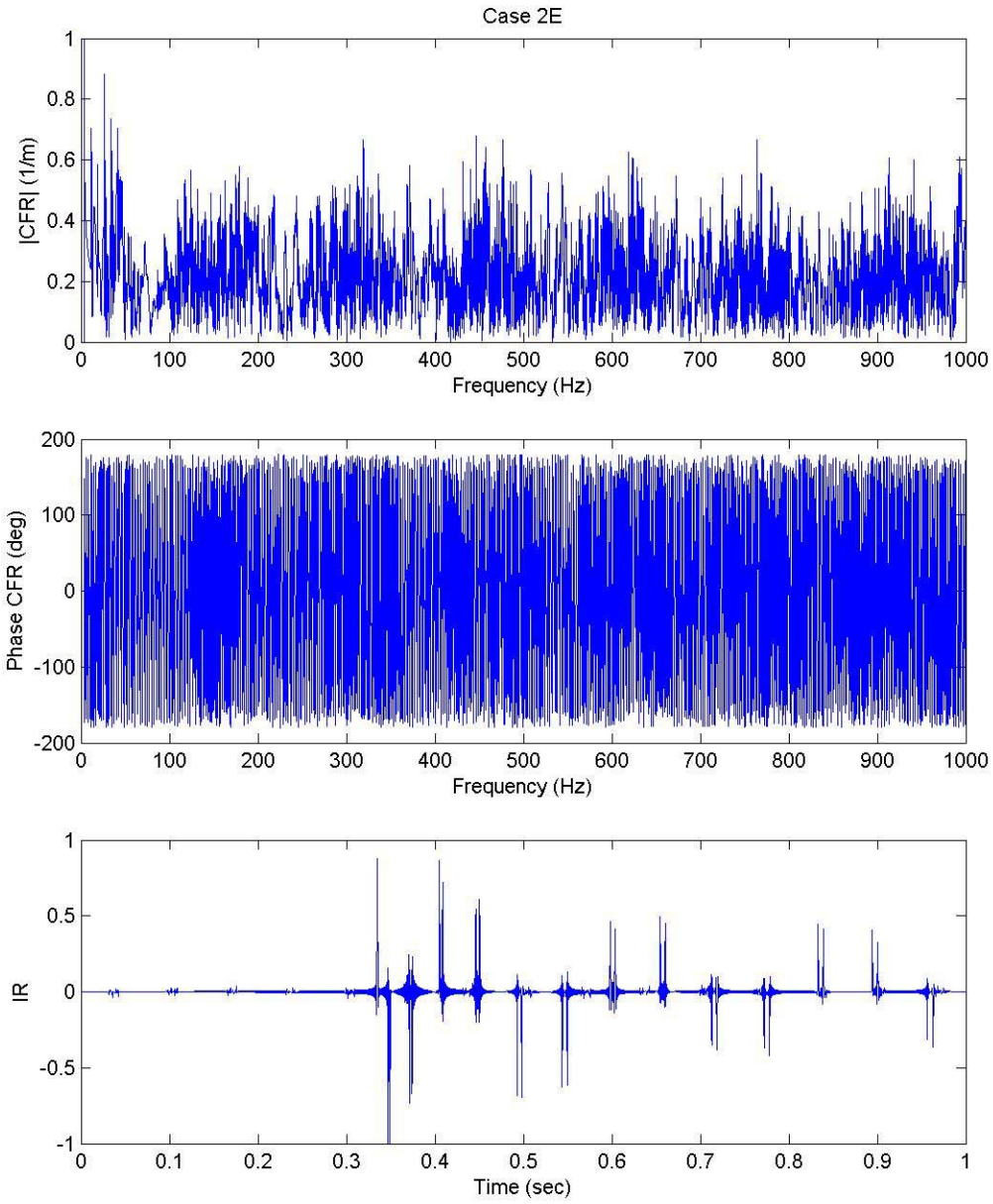

Figure 3.16. Magnitude and phase of complex frequency response (CFR) and impulse response (IR) for Case 2E.

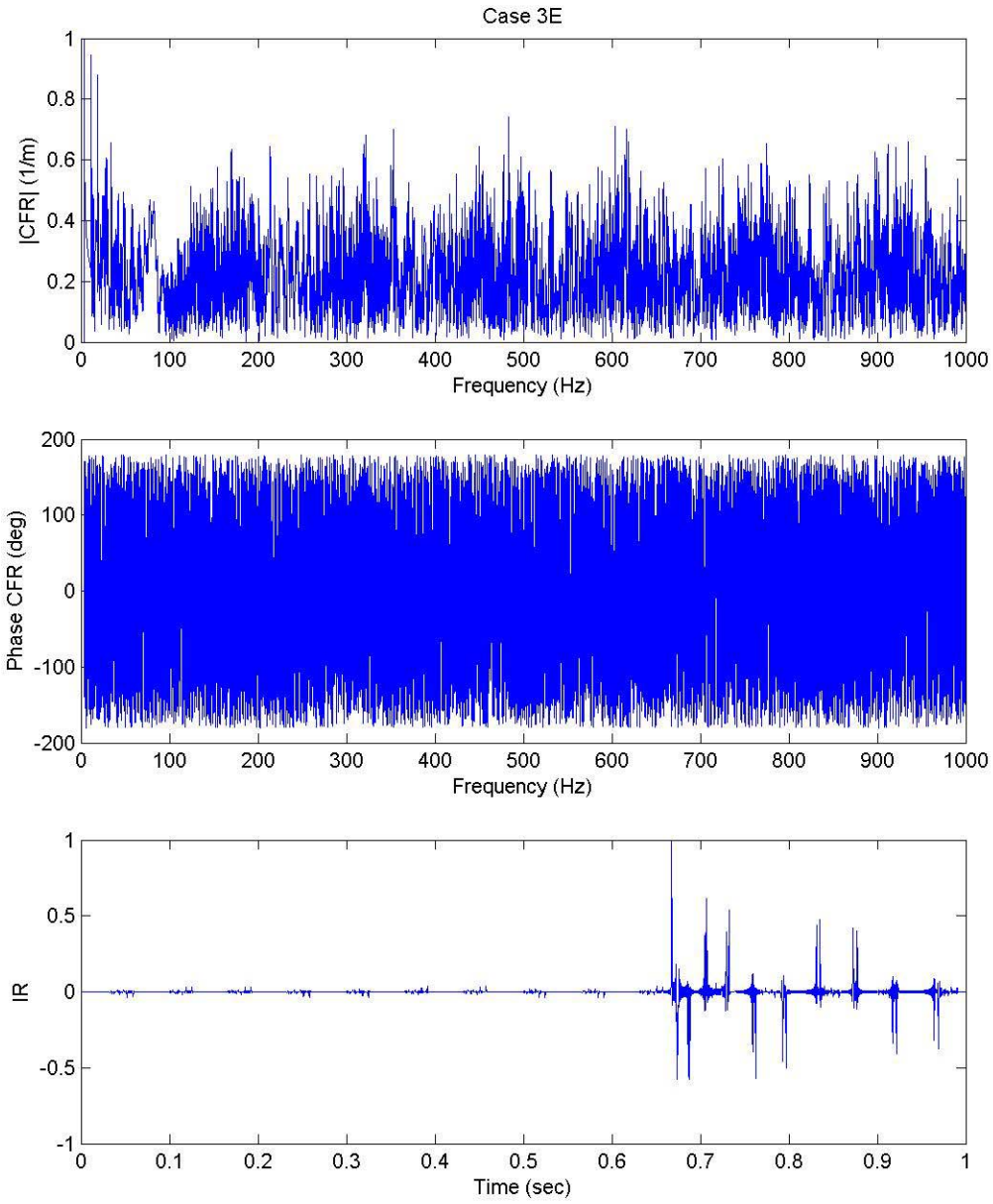

Figure 3.17. Magnitude and phase of complex frequency response (CFR) and impulse response (IR) for Case 3E.

E. TRANSFER FUNCTION OF THE OCEAN

Having demonstrated the usefulness of the impulse response in determining range-to-target and positive or negative depth offset, it is now necessary to demonstrate the usefulness of the transfer function of the ocean with respect to depth. This can best be done graphically. For each of the cases, source depth is not used to evaluate the transfer function. The mathematics of the transfer function equation require only that the receiver depth be used [see (2.40)]. The magnitude of the transfer function shows how the ocean responds to different launch angles β_0 at the source. The test cases used to evaluate the transfer function are summarized in Table 3.7.

	A	B	C
1	$r = 300$ m $y = 5$ m	$r = 300$ m $y = 50$ m	$r = 300$ m $y = 95$ m
2	$r = 500$ m $y = 5$ m	$r = 500$ m $y = 50$ m	$r = 500$ m $y = 95$ m
3	$r = 1000$ m $y = 5$ m	$r = 1000$ m $y = 50$ m	$r = 1000$ m $y = 95$ m

Table 3.7. Transfer function test cases

The transfer functions for the preceding nine test cases were evaluated to demonstrate their dependence on frequency, range and receiver depth. An inspection of (2.40) will reveal that the transfer function changes the most with a change in frequency. This is due to the fact that the spatial frequency f_Y depends on frequency as launch angle β_0 is varied from 0° to 90°. Subsequently, the $\text{sinc}(\bullet)$ function in (2.40) also depends on frequency. As was the case with the complex frequency response, the Hankel function in (2.40) varies with frequency and horizontal range, and the sinusoid depends on the receiver depth *y*. Unfortunately, there does not appear to be an observable trend as any of the variables (f, r, y) is increased or decreased. To illustrate this fact, the transfer function for cases 'A' are shown for source frequencies of 250, 500, 750, and 1000 Hz,

respectively, as Figs. 3.20 through 3.22. The magnitudes of the transfer function are normalized to observe launch angle dependence.

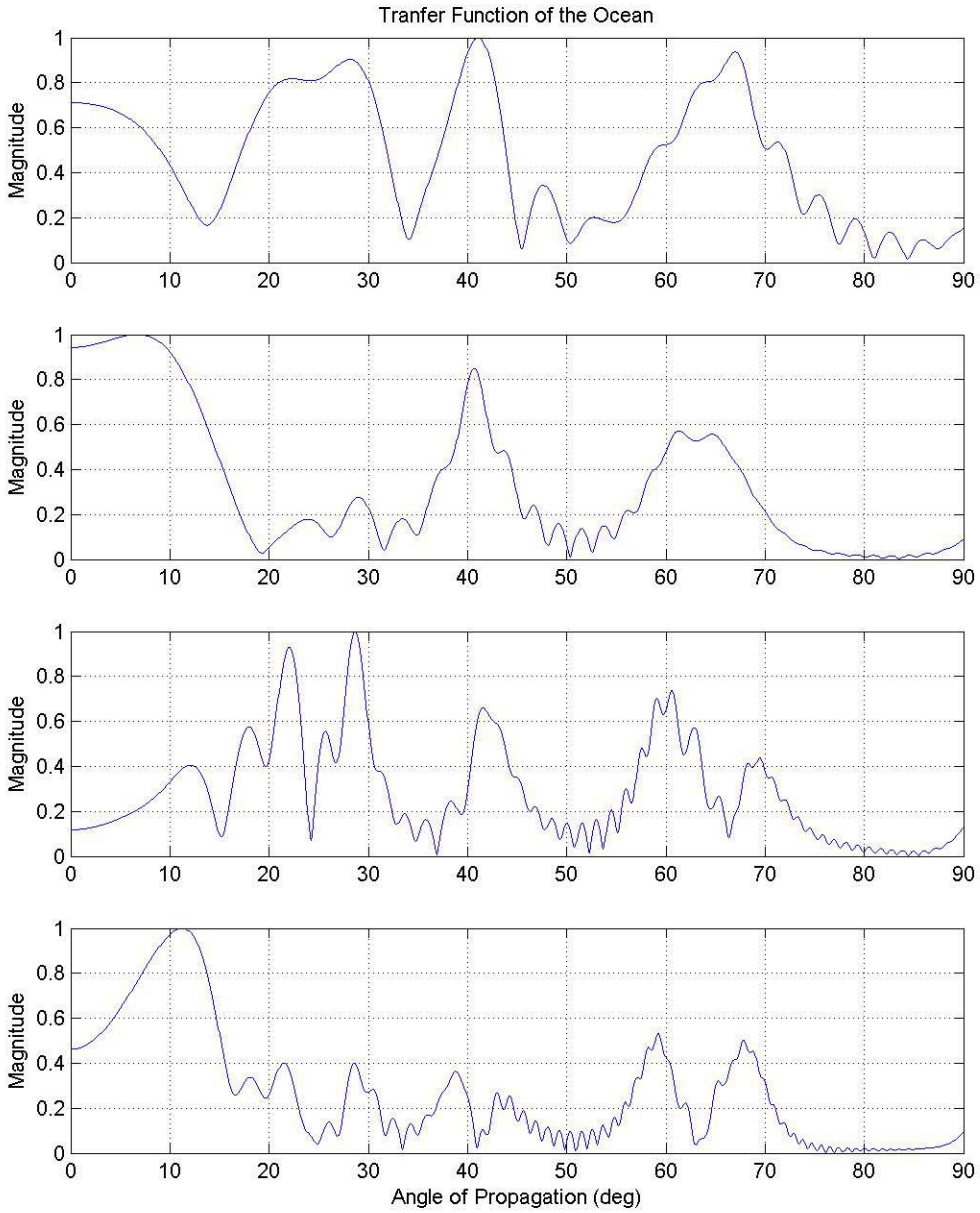

Figure 3.18. Case 1A, 250, 500, 750, and 1000 Hz

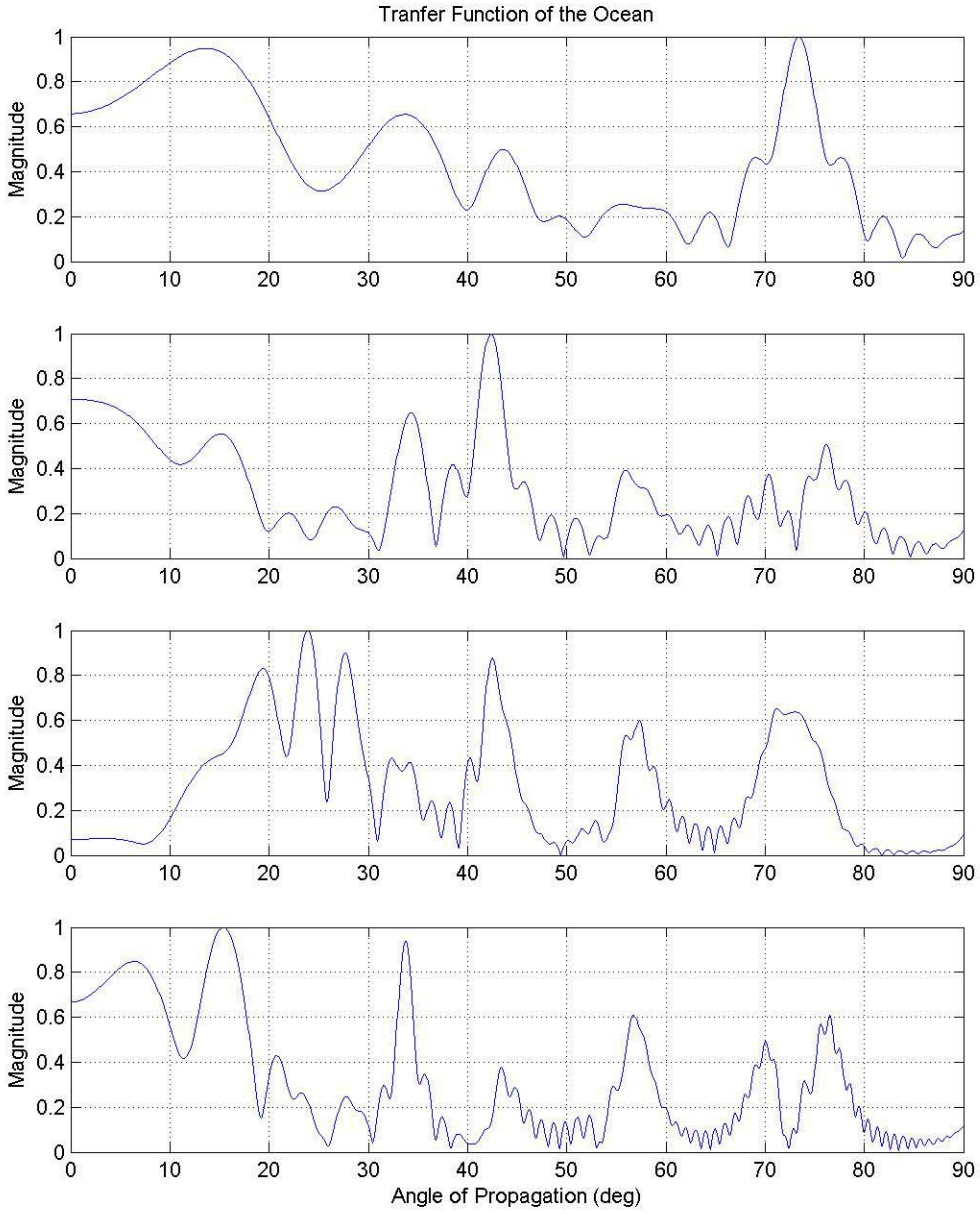

Figure 3.19. Case 2A, 250, 500, 750, and 1000 Hz

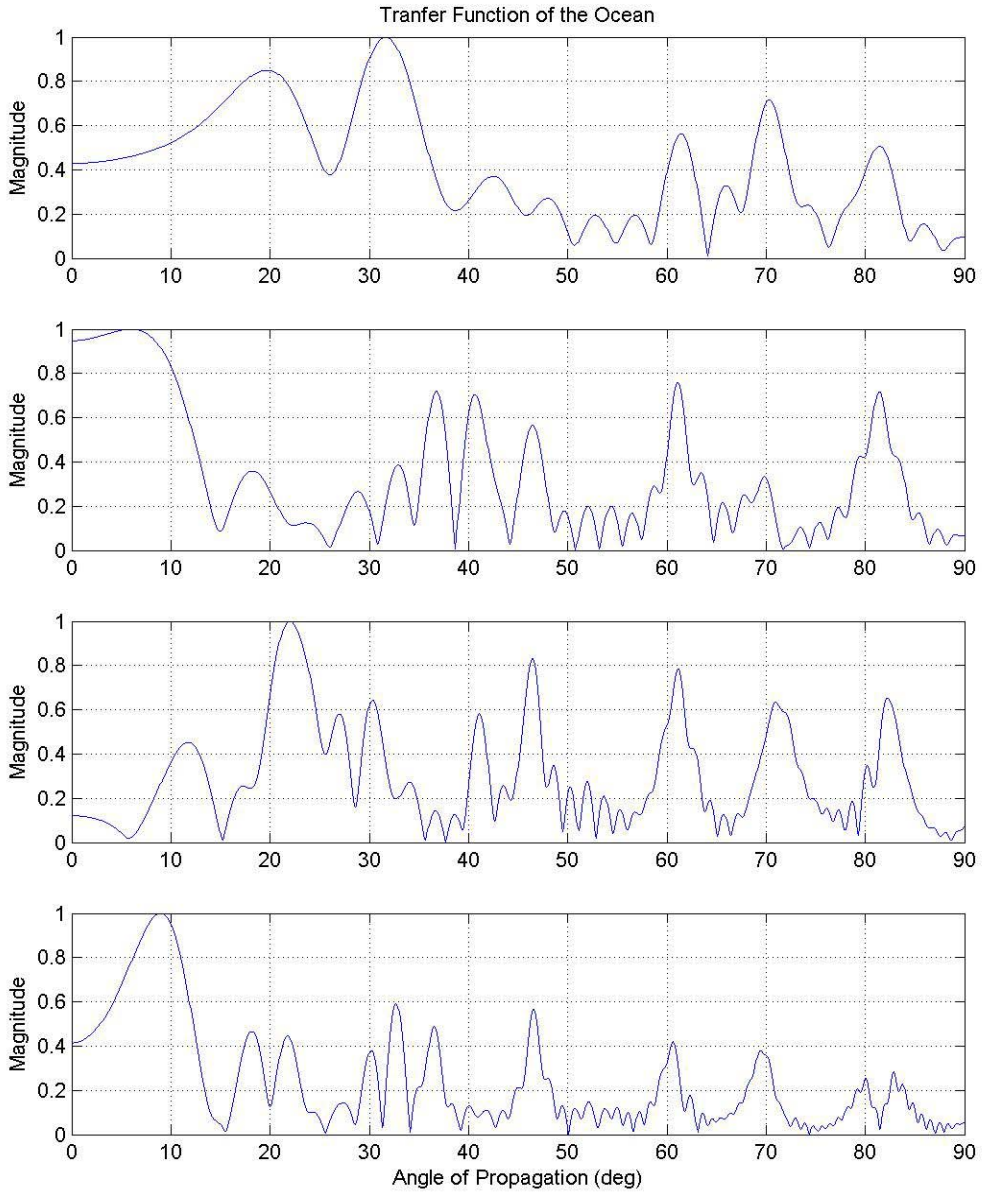

Figure 3.20. Case 3A, 250, 500, 750, and 1000 Hz

Now that the lack of a general trend for increases in frequency has been established, the rest of the test cases will be shown for 250 Hz only. Cases 'B' and 'C' are shown in order of increasing range as Figs. 3.23 through 3.28. These figures show how the ocean responds to different launch angles (angles of propagation) β_0 at the source.

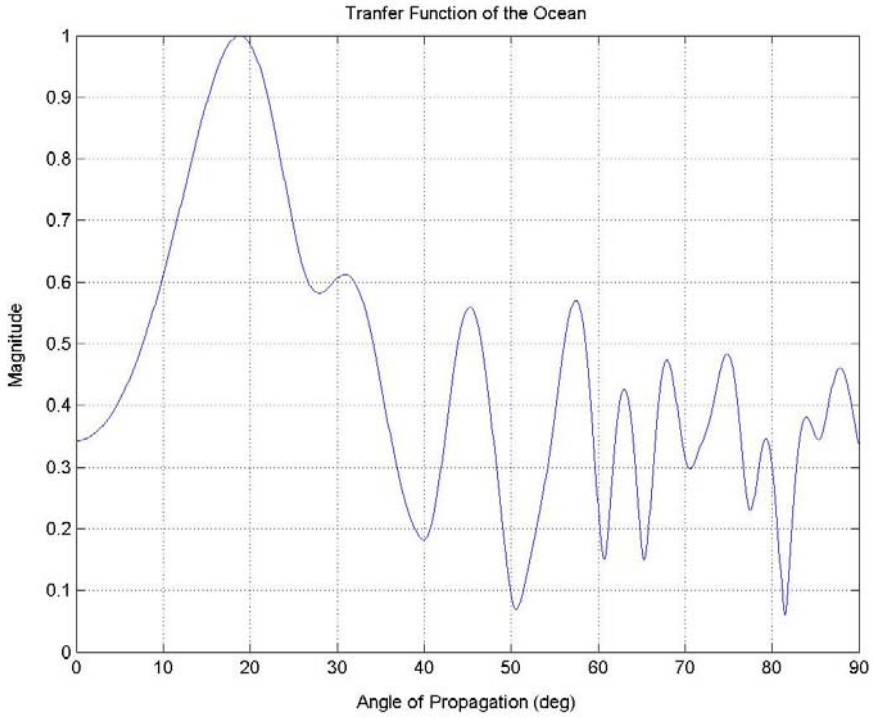

Figure 3.21. Case 1B

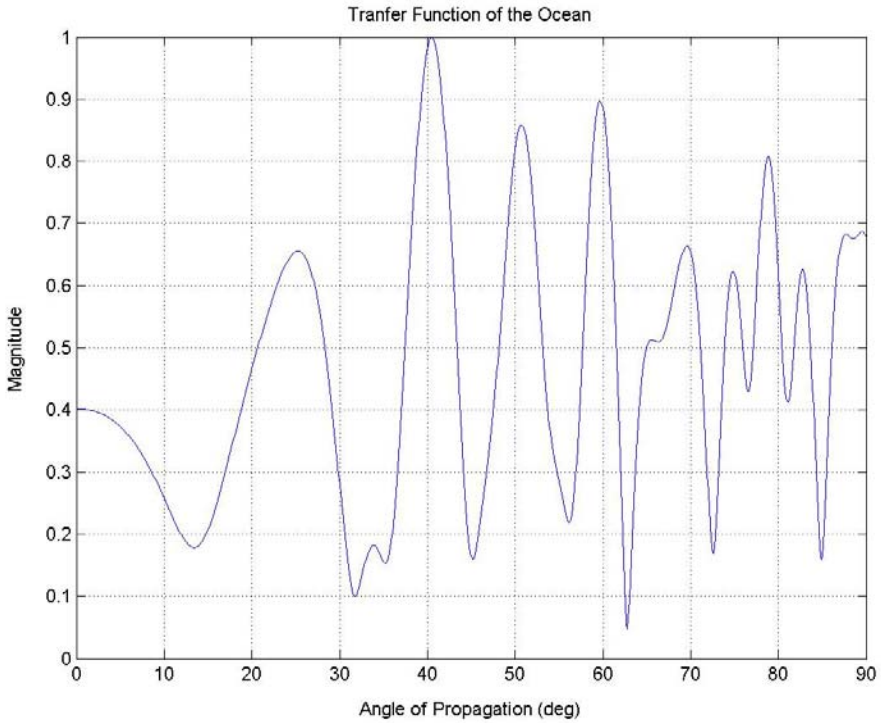

Figure 3.22. Case 2B

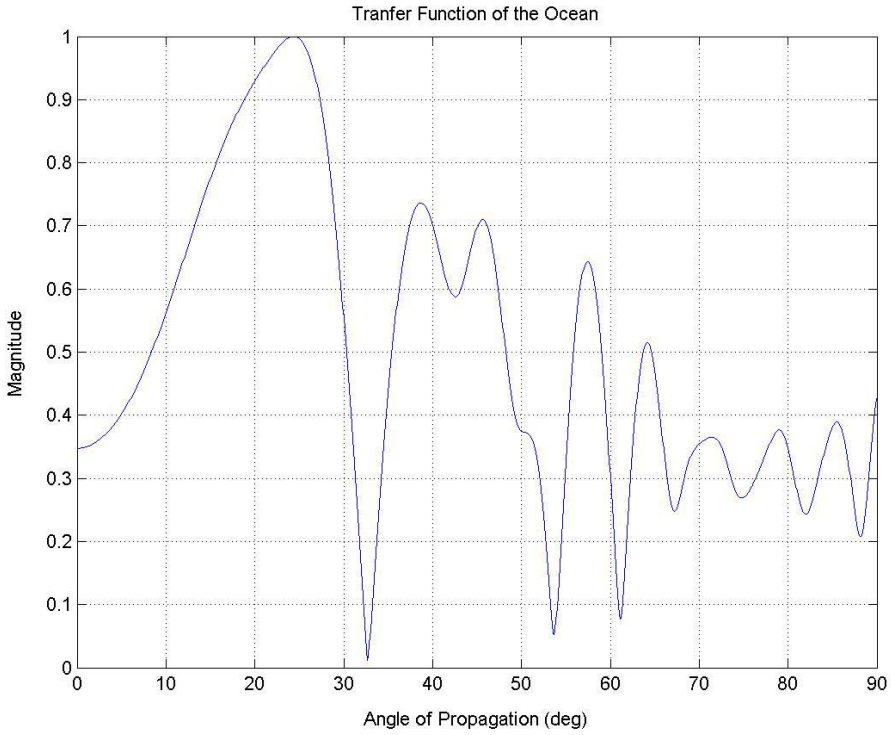

Figure 2.23. Case 3B

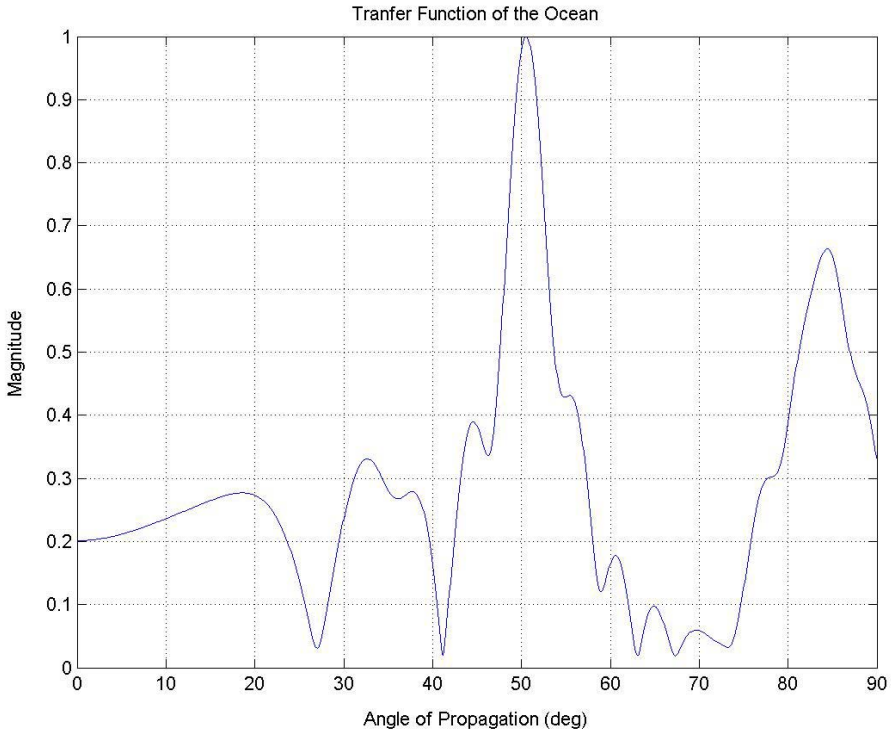

Figure 3.24. Case 1C

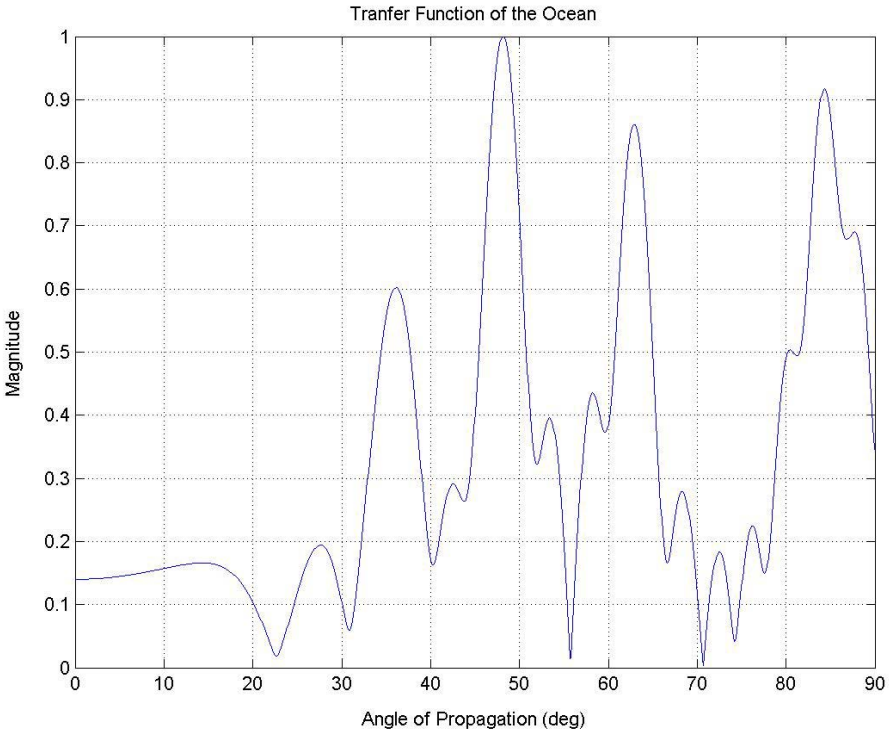

Figure 3.25. Case 2C

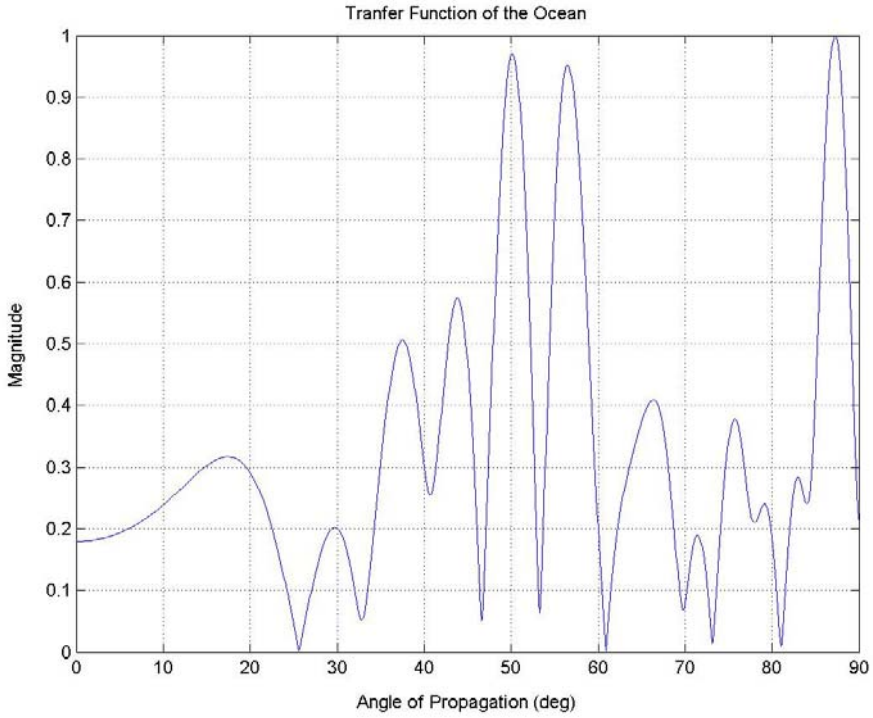

Figure 3.26. Case 3C

THIS PAGE INTENTIONALLY LEFT BLANK

IV. CONCLUSIONS

A. SUMMARY OF RESULTS

In Chapter III, we effectively demonstrated that a time – invariant, space – variant (TISV) impulse response could be derived from a TISV complex frequency response using an inverse discrete Fourier transform (IDFT). We further demonstrated that this impulse response could be used to determine approximate horizontal range – to – target and whether the target was above, below, at the same depth as the receiver. Finally, we showed that the TISV transfer function with respect to depth could be used to determine which launch angle from the target would produce the maximum magnitude response of the transfer function.

B. POSSIBLE EMPLOYMENT SCENARIO

Shallow water presents unique problems to both active and passive sonar systems due to multi – path propagation. If the complex frequency response of the ocean can be estimated in real time, and if it can be treated as being time – invariant during the period of operation of a sonar system, then it can be used to compute the impulse response of the ocean using an IDFT. This impulse response would yield a fairly accurate range – to – target estimate and whether the target is above or below the sonar system.

C. RECOMMENDATIONS FOR FUTURE RESEARCH

Since the time – invariant, space – variant impulse response contains information about the *nature* of the depth offset between the source (target) and receiver, future study should determine if it contains information about the *size* of the offset, as was the case with range. If the amount of depth offset (positive or negative) could be estimated, this information together with the range estimate would be enough to localize the sound source.

The waveguide model used in this thesis was based on the assumption of an ideal rigid bottom. The fast bottom model described in Ziomek [6] should be explored since it is a more realistic model. Taking into account the effects of attenuation in both the ocean medium and ocean bottom should also be explored.

The transfer function equation was derived to give information about the response of the ocean for a given launch angle *from the source*. The transfer function should be re-derived with respect to receiver depth to give information about the response of the ocean for a given angle of arrival *at the receiver*.

Lastly, for practical purposes, the MATLAB code used to compute our numerical results should be rewritten in JAVA or another compiled language in order to make faster calculations.

LIST OF REFERENCES

1. Ellinthorpe, A.W. and A.H. Nuttall, "Theoretical and empirical results on the characterization of undersea acoustic channels," IEEE First Annual Communication Convention, 1965.

2. Middlteon, D., "A Statistical theory of reverberation and similar first-order scattered fields. Part I: Waveforms and the general process," IEEE *Trans. Inf. Theory,* **IT-13**, 372-392 (1967).

3. Sostrand, K. A., "Mathematics of the time-varying channel," in *Proceedings of the NATO Advanced Study Institute on Signal Processing with emphasis on underwater acoustics*, Vol. II, Enschede, The Netherlands, 1968.

4. Laval, R., "Sound propagation effects on signal processing," in *Signal Processing*, (edited by J.W.R Griffiths, P.L. Stocklin, and C. Van Schooneveld), Academic Press, New York, 1973.

5. Laval, R., "Time-frequency-space generalized coherence and scattering functions," in *Aspects of Signal Processing*, Part I, (edited by G. Tacconi), D. Reidel, Dordrecht, Holland, 1977.

6. Ziomek, L.J., "Pulse propagation and bistatic scattering," Technical Report No. NPS-EC-02-001, Naval Postgraduate School, Monterey, California, October 2001.

7. Ziomek, L.J., *Fundamentals of Acoustic Field Theory and Space – Time Signal Processing*, CRC Press, Boca Raton, Florida, 1995, pp. 211, 213.

THIS PAGE INTENTIONALLY LEFT BLANK

INITIAL DISTRIBUTION LIST

1. Defense Technical Information Center
   Ft. Belvoir, Virginia

2. Dudley Knox Library
   Naval Postgraduate School
   Monterey, California

3. Dr. Lawrence J. Ziomek
   Naval Postgraduate School
   Monterey, CA

4. Dr. Roberto Cristi
   Naval Postgraduate School
   Monterey, CA

5. Dr. Donald Brutzman
   Chair of USW/Academic Committee
   Naval Postgraduate School
   Monterey, CA

6. N-75, Director Expeditionary Warfare Division
   Chief of Naval Operations
   Washington, D.C.

7. N-77, Director Submarine Warfare Division
   Chief of Naval Operations
   Washington, D.C.

8. Fleet ASW Command
   San Diego, CA

9. Commander Submarine Development Squadron Twelve
   Naval Submarine Base
   Groton, CT

10. Commander Third Fleet
    ATTN: Naval Postgraduate School Representative
    FPO AP 96601 –6001

11. Office of Naval Research
    Ocean, Atmosphere and Space Department
    ONR Code 32
    Arlington, VA